Geophys. J. R. astr. Soc. (1984) **76**, 753–791

Pleistocene deglaciation and the Earth's rotation: a new analysis

Patrick Wu and W. R. Peltier *Department of Physics, University of Toronto, Toronto, Ontario M5S 1A7, Canada*

Received 1983 September 5; in original form 1982 October 25

Summary. This paper is concerned with an analysis of the effect of the Pleistocene glacial cycle upon the Earth's rotation. We demonstrate that two important geophysical observables may be explained as aspects of the rotational response to surface mass loading by ice sheets. These are the astronomically observed non-tidal component of the acceleration of planetary rotation and the secular drift of the rotation pole relative to the surface geography which is evident in the ILS pole path. The former observation is shown to provide an unambiguous constraint upon the viscosity of the planetary mantle and requires a depth dependence of this parameter which is the same as that which has previously been inferred in studies of the relative sea-level variations and free air gravity anomalies associated with post-glacial rebound. The observed secular drift of the pole cannot provide an independent estimate of the viscosity of the mantle because it depends jointly upon mantle viscosity and lithospheric thickness. With the viscosity profile fixed by the rebound data, the observed speed of polar wander suggests a continental lithospheric thickness which is in excess of that appropriate for old ocean basins but nevertheless in accord with independent constraints.

1 Introduction

The inference of mantle viscosity through analysis of effects associated with the melting of large continental ice masses provides the only method by which direct estimates of this parameter may be obtained. Until quite recently, the only such observations to be employed with consistent success were those concerned with the variations of relative sea-level which were forced by the final melting of Würm–Wisconsin ice which began about 18 000 yr ago (e.g. Peltier 1981). In the past few years one additional datum, the free air gravity anomalies observed over the main centres of rebound, has been shown to provide an estimate of mantle viscosity which is consistent with that implied by the relative sea-level data (Peltier 1981; Peltier & Wu 1982; Wu & Peltier 1983). This datum was shown to be particularly useful because it increased our ability to resolve the variations of viscosity through the transition region from 420 to 670 km depth. The combined data have been shown to require

a modest increase of viscosity between the upper and lower mantles of about a factor of 3. This result is important because it shows that there is no purely mechanical impediment to convection through this region as has often been assumed in the past (e.g. McKenzie 1967; McKenzie & Weiss 1975). As argued in Peltier & Jarvis (1982) and Peltier (1982), unless there are effects due to the phase change at 670 km depth which are such as to inhibit convection, or unless this boundary is at least in some significant part a chemical boundary, then convection should be whole mantle in scale. The observation that the viscosity of the mantle does not change significantly across the spinel–post-spinel phase change is therefore an important constraint upon models of mantle mixing.

Because this result is an important one, we have recently been attempting to discover whether there might not be other geophysical data which could provide an even further increase of our ability to resolve the depth variation of viscosity and to provide further corrobation of these inferences. One avenue of investigation which we thought might yield the desired information, and which we have previously explored in at least a tentative fashion, concerns effects upon the Earth's rotation which might be produced by ice sheet accumulation and disintegration. Our initial exploration of this possibility (Sabadini & Peltier 1981; hereafter SP) led us to the conclusion that both the observed non-tidal acceleration of the Earth's rotation and the observed secular drift in the ILS pole path were due to deglacial forcing. In SP we employed a homogeneous viscoelastic model of the Earth to fit the two observations and found that we could fit the two rotation data when the mantle viscosity was chosen to be near that implied by the rsl and free air gravity data.

An independent analysis of the problem of deglaciation forced polar motion was produced concurrently by Nakiboglu & Lambeck (1980, 1981, hereafter NL). Although these authors came essentially to the same conclusion as SP, and their earth model was the same homogeneous model as that employed by SP, the two calculations differed significantly in the assumptions made concerning the glaciation history and in the approximations made in solving the equations of rotational dynamics. A detailed comparison of these two independent analyses has shown each to contain a serious flaw which undermines the conclusions to which their authors were led. The purpose of this paper is to summarize the analyses through which we have reached this conclusion and to provide a reassessment of the hypothesis that the two rotational effects both have a deglacial cause and can be employed to constrain the viscoelastic stratification of the Earth. As we will show, our original hypothesis is only reconfirmed by the new analysis. The dependence of the theoretical predictions of the more accurate model upon the model parameters, however, is such as to require several significant modifications of the conclusions reached previously.

In Section 2 we provide the general theoretical background required to understand the problem of deglaciation-forced rotational effects. Although some of this material is similar to that provided in SP, at several points in the present analysis we are able to provide more general derivations of results obtained in SP by somewhat clumsier means. We have also extended the theory to encompass much more realistic deglaciation histories than those employed previously. Section 3 contains a detailed analysis of deglaciation-forced polar wander both for homogeneous and for realistic stratified viscoelastic models of the planet. Section 4 is concerned with the question of the acceleration of rotation which is produced by ice sheet ablation and accumulation. In this section we also point to the possibility, unrecognized previously, that there might be another geophysical observable which is intimately related to the acceleration of rotation and which could be employed as a further check upon the mantle viscosity inferred from this datum. This new observable concerns the time derivative of the second-degree component of the Earth's gravitational potential field. Since the parameter J_2 may be very accurately measured by observing the precession rates of the orbital planes of artificial earth satellites, its time derivative may be estimated from the J_2

time series. Our analysis slows that this measurement has become feasible with the advent of modern satellite laser ranging technology.

2 Theory of the rotational response to surface loading

Since the aquasphere, cryosphere, solid earth system is subjected to no significant external torque during the course of the climatic changes associated with the accumulation and disintegration of Pleistocene ice sheets, the angular momentum of the total system is conserved. The variations of system angular velocity $\boldsymbol{\omega}$ are therefore governed by the usual Euler equations of classical mechanics which may be written in the form

$$\frac{d}{dt}(J_{ij}\omega_j) + \epsilon_{ijk}\omega_j J_{kl}\omega_l = 0, \tag{1}$$

in which J_{ij} is the moment of inertia tensor and ϵ_{ijk} the Levi-Cevita (alternating) tensor. Although the system of equations (1) is highly non-linear in general, a linearized version of (1) provides an accurate description of the rotational motion as long as the instantaneous position of the rotation pole does not deviate substantially from some reference position. We shall assume, as is conventional, a coordinate system which is fixed to the rotating Earth with its origin at the Earth's centre of mass (COM) and oriented such that the inertia tensor of the initially unperturbed Earth is diagonal. Equation (1) may then be linearized with the following perturbation expansion

$$\omega_i = \Omega(\delta_{i3} + m_i) \tag{2}$$

$$J_{ij} = I_{ij} \qquad i \neq j \tag{3}$$

$$J_{11} = A + I_{11}$$

$$J_{22} = A + I_{22}$$

$$J_{33} = C + I_{33}$$

in which (A, A, C) are the principal moments of inertia, Ω is the initial (mean) angular velocity of the Earth, and I_{ij} and m_i are small fluctuations away from the basic state values.

When equations (2) and (3) are substituted in (1) and all terms dropped which are of second order or higher in the smaller fluctuations then (1) decouples to the following two equations

$$\frac{i}{\sigma_r}\dot{\mathbf{m}} + \mathbf{m} = \psi \tag{4}$$

$$\dot{m}_3 = \dot{\psi}_3 \tag{5}$$

which are called Liouville's equations by Munk & MacDonald (1960). In (4) the parameter σ_r is the Chandler wobble frequency of the rigid earth,

$$\sigma_r = \Omega\frac{(C-A)}{A}, \tag{6}$$

and the vectors $\mathbf{m}$ and ψ are such that

$$\mathbf{m} = m_1 + im_2 \tag{7a}$$

$$\psi = \psi_1 + i\psi_2 \tag{7b}$$

$$\psi_1 = \frac{I_{13}}{(C-A)} + \frac{\dot{I}_{23}}{\Omega(C-A)} \tag{8a}$$

$$\psi_2 = \frac{I_{23}}{(C-A)} - \frac{\dot{I}_{13}}{\Omega(C-A)} \tag{8b}$$

$$\psi_3 = -\frac{I_{33}}{C}. \tag{8c}$$

The parameters ψ_i are components of the rotational excitation function. Inspection of equations (4), (5) and (8) shows that the unknown m_i are determined completely by the perturbations of the inertia tensor I_{13}, I_{23}, I_{33}. In order to solve (4) and (5) we must first determine these perturbations and they each contain contributions from two sources. The first is that associated with the redistribution of glacial ice and water on the Earth's surface and with the redistribution of mass in the planetary interior which these surface mass loads induce. The second contribution is that due to the deformation of the planet associated with the changing rotation itself. These two contributions are discussed in the following subsections.

2.1 PERTURBATIONS OF INERTIA DUE TO SURFACE LOADING

We will divide this discussion into two parts, since it is of some tutorial advantage to discuss separately perturbations of inertia due to the direct effect of the loads and those due to the associated internal redistribution of mass.

2.1.1 Inertia perturbations due to the direct effect of the load

The perturbations of inertia due to extra mass of density $\rho(\mathbf{x})$ are by definition

$$I_{ij}^{\mathrm{R}} = \int_a^{a+h} \int_s \int \rho(\mathbf{x})(x_r x_r \delta_{ij} - x_i x_j)\, ds\, dr \tag{9}$$

where a is the Earth's mean radius and h is the topographic height of the load. Since $h/a \ll 1$ we can treat $\rho(\mathbf{x})$ as a surface mass density $\sigma(a, \theta, \phi)$ without incurring significant error to obtain

$$I_{ij}^{\mathrm{R}} = \int_s \int \sigma(\theta, \phi)(a^2 \delta_{ij} - x_i x_j)\, ds. \tag{10}$$

It is convenient to expand $\sigma(\theta, \phi)$ into spherical harmonics, as

$$\sigma(\theta, \phi) = \sum_{n=0}^{\infty} \sum_{m=0}^{n} (\sigma_{nm1} \cos m\phi + \sigma_{nm2} \sin m\phi) P_n^m(\cos\theta) \tag{11}$$

in which P_n^m are the usual (un-normalized) associated Legendre functions which have the property

$$\int\int [P_n^m(\cos\theta) \begin{matrix}\cos m\phi \\ \sin m\phi\end{matrix}]^2\, ds = \frac{4\pi(n+m)!}{(2n+1)(n-m)!(2-\delta_{om})}. \tag{12}$$

Substitution of (11) into (10) and application of (12) then yields

$$I_{13}^{\mathrm{R}} = -\tfrac{4}{5}\pi a^4 \sigma_{211} \tag{13a}$$

$$I_{23}^{\mathrm{R}} = -\tfrac{4}{5}\pi a^4 \sigma_{212} \tag{13b}$$

$$I_{33}^{\mathrm{R}} = \tfrac{8}{3}\pi a^4 \left[\sigma_{001} - \frac{\sigma_{201}}{5}\right]. \tag{13c}$$

It should be clear that the σ_{nmi} are dependent upon the geometry of the ice sheets and the oceans into which they discharge their meltwater. In the remainder of this subsection we

will consider a few examples of $\sigma(\theta, \phi)$ which will be useful in our later discussion. In each case considered we will assume that the total mass is conserved so that the average of $\sigma(\theta, \phi)$ is always identically zero. We will also restrict consideration to cases in which the ice is uniformly distributed within fixed boundaries and in which the water is uniformly distributed within similarly fixed oceans.

Case (*i*) $\sigma(\theta, \phi)$ for a single circular ice cap

If the total mass of the ice cap at time t is $M(t)$ and if the cap is located on the pole and has radius α then as in SP we have

$$\sigma_{\mathrm{ICE}}(\theta) = \frac{M}{4\pi a^2}\left[P_n^0(\cos\theta) + \sum_{n=1}^{\infty} \frac{(2n+1)(1+\cos\alpha)}{n(n+1)} \frac{\partial P_n(\cos\alpha)}{\partial \cos\alpha} P_n^0(\cos\theta)\right]. \tag{14}$$

If this cap is located at colatitude θ' and east longitude ϕ' we can use the addition theorem for spherical harmonics in the form

$$P_n^0(\cos\gamma) = P_n^0(\cos\theta')\, P_n^0(\cos\theta) + 2\sum_{m=1}^{n} \frac{(n-m)!}{(n+m)!} P_n^m(\cos\theta')\, P_n^m(\cos\theta)\cos m(\phi - \phi') \tag{15}$$

where

$$\cos\gamma = \cos\theta'\cos\theta + \sin\theta'\sin\theta\cos(\phi - \phi')$$

to write

$$\begin{aligned}\sigma_{\mathrm{ICE}}(\theta, \phi) = {} & \frac{M}{4\pi a^2} + \sum_{m=1}^{\infty}\left[\frac{M}{4\pi a^2}\frac{(2n+1)(1+\cos\alpha)}{n(n+1)}\frac{\partial P_n^0(\cos\alpha)}{\partial\cos\alpha}P_n^0(\cos\theta')\right]P_n^0(\cos\theta) \\ & + \sum_{n=1}^{\infty}\sum_{m=1}^{n}\left[\frac{M}{2\pi a^2}\frac{(2n+1)(1+\cos\alpha)(n-m)!}{n(n+1)(n+m)!}\frac{\partial P_n^0(\cos\alpha)}{\partial\cos\alpha}P_n^m(\cos\theta')\right] \\ & \times [\cos m\phi'\cos m\phi + \sin m\phi'\sin m\phi]\, P_n^m(\cos\theta).\end{aligned} \tag{16}$$

Case (*ii*) $\sigma(\theta, \phi)$ for a complementary circular ocean

If the ocean is everywhere outside the circular ice cap of case (i) whose centre is at (θ', ϕ') then the surface mass density of this simplified ocean is as in SP

$$\begin{aligned}\sigma_{\mathrm{OC}}(\theta, \phi) = {} & -\frac{M}{4\pi a^2} + \sum_{n=1}^{\infty}\left[\frac{M}{4\pi a^2}\frac{(2n+1)(1-\cos\alpha)}{n(n+1)}\frac{\partial P_n^0(\cos\alpha)}{\partial\cos\alpha}P_n^0(\cos\theta')\right]P_n^0(\cos\theta) \\ & + \sum_{n=1}^{\infty}\sum_{m=1}^{n}\left[\frac{M}{2\pi a^2}\frac{(2n+1)(1-\cos\alpha)}{n(n+1)}\frac{(n-m)!}{(n+m)!}\frac{P_n^0(\cos\alpha)}{\partial\cos\alpha}P_n^m(\cos\theta')\right] \\ & \times [\cos m\phi'\cos m\phi + \sin m\phi'\sin m\phi]\, P_n^m(\cos\theta).\end{aligned} \tag{17}$$

Combining cases (i) and (ii) we may write for the total system

$$\begin{aligned}\sigma(\theta, \phi) = {} & \sigma_{\mathrm{ICE}} + \sigma_{\mathrm{OC}} \\ = {} & \sum_{n=1}^{\infty}\left[\frac{M}{2\pi a^2}\frac{(2n+1)}{n(n+1)}\cdot\frac{\partial P_n(\cos\alpha)}{\partial\cos\alpha}P_n(\cos\theta')\right]P_n(\cos\theta) \\ & + \sum_{n=1}^{\infty}\sum_{m=1}^{n}\left[\frac{M}{\pi a^2}\frac{(2n+1)(n-m)!}{n(n+1)(n+m)!}\frac{\partial P_n(\cos\alpha)}{\partial\cos\alpha}P_n^m(\cos\theta')\right] \\ & \times [\cos m\phi'\cos m\phi + \sin m\phi'\sin m\phi]\, P_n^m(\cos\theta)\end{aligned} \tag{18}$$

from which we may extract

$$\sigma_{001} = 0$$

$$\sigma_{201} = \frac{5M\cos\alpha}{4\pi a^2} P_2^0(\cos\theta^1)$$

$$\sigma_{211} = \frac{5M\cos\alpha}{12\pi a^2} \cos\phi' P_2^1(\cos\theta') = -\frac{5M\cos\alpha}{4\pi a^2} \cos\phi' \cos\theta' \sin\theta' \tag{19}$$

$$\sigma_{212} = \frac{5M\cos\alpha}{12\pi a^2} \sin\phi' P_2^1(\cos\theta') = -\frac{5M\cos\alpha}{4\pi a^2} \sin\phi' \cos\theta' \sin\theta'$$

which are required in (13) to determine the perturbations of inertia.

Case (iii) $\sigma(\theta, \phi)$ for a realistic ocean

The surface mass density for a mass M distributed uniformly over a geographically realistic global ocean may be written as

$$\sigma_{\mathrm{OCEAN}}(\theta, \phi) = -\frac{M}{A_0} \zeta(\theta, \phi) \tag{20}$$

where $\zeta(\theta, \phi)$ is the so-called ocean function (Munk & MacDonald 1960; Lambeck 1980) which has the following spherical harmonic decomposition

$$\zeta(\theta, \phi) = a_{00} + \sum_{n=1}^{\infty} \sum_{m=0}^{n} (a_{nm} \cos m\phi + b_{nm} \sin m\phi) P_n^m(\cos\theta) \tag{21}$$

and A_0 is the total area of the ocean floor such that

$$A_0 = \iint \zeta(\theta, \phi) a^2 \sin\theta \, d\theta \, d\phi = 4\pi a^2 a_{00}. \tag{22}$$

Equation (20) may therefore be rewritten as

$$\sigma_{\mathrm{OCEAN}}(\theta, \phi) = -\frac{M}{4\pi a^2} - \frac{M}{4\pi a^2} \sum_{n=1}^{\infty} \sum_{m=0}^{n} \left(\frac{a_{nm}}{a_{00}} \cos m\phi + \frac{b_{nm}}{a_{00}} \sin m\phi \right) P_n^m(\cos\theta). \tag{23}$$

If this realistic ocean were fed from a single circular ice cap centred on colatitude θ' and east longitude ϕ' then the net surface mass density for this load would be

$$\sigma(\theta, \phi) = \sigma_{\mathrm{ICE}} + \sigma_{\mathrm{OCEAN}}$$

$$= \sum_{n=1}^{\infty} \sum_{m=0}^{n} (\sigma_{nm1} \cos m\phi + \sigma_{nm2} \sin m\phi) P_n^m(\cos\theta) \tag{24}$$

with

$$\sigma_{001} = 0$$

$$\sigma_{n01} = \frac{M}{4\pi a^2} \left[\frac{(2n+1)(1+\cos\alpha)}{n(n+1)} \frac{\partial P_n(\cos\alpha)}{\partial \cos\alpha} P_n(\cos\theta') - \frac{a_{n0}}{a_{00}} \right]$$

$$\sigma_{nm1} = \frac{M}{4\pi a^2} \left[\frac{2(n-m)!}{(n+m)!} \frac{(2n+1)(1+\cos\alpha)}{n(n+1)} \frac{\partial P_n(\cos\alpha)}{\partial \cos\alpha} P_n^m(\cos\theta') \cos(m\phi') - \frac{a_{nm}}{a_{00}} \right] \tag{25}$$

$$\sigma_{nm2} = \frac{M}{4\pi a^2} \left[\frac{2(n-m)!}{(n-m)!} \frac{(2n+1)(1+\cos\alpha)}{n(n+1)} \frac{\partial P_n(\cos\alpha)}{\partial \cos\alpha} P_n^m(\cos\theta') \sin(m\phi') - \frac{b_{nm}}{a_{00}} \right].$$

From equations (25) we may extract the coefficients required to compute the perturbations of the inertia tensor according to (13). These are then

$$I_{13}^{R} = Ma^2 \left[\tfrac{1}{6} \cos\alpha(1+\cos\alpha) P_2^1(\cos\theta') \cos\phi' \right] \cos\phi' - \frac{a_{21}}{5a_{00}}$$

$$I_{23}^{R} = Ma^2 \left[\tfrac{1}{6} \cos\alpha(1+\cos\alpha) P_2^1(\cos\theta') \sin\phi' - \frac{b_{21}}{5a_{00}} \right] \tag{26}$$

$$I_{33}^{R} = Ma^2 \left[\tfrac{2}{15} \frac{a_{20}}{a_{00}} - \frac{\cos\alpha(1+\cos\alpha)}{3} P_2^0(\cos\vartheta') \right].$$

Using the data tabulated in Lambeck (1980) we have

$$\frac{a_{20}}{a_{00}} = \sqrt{5}\left(\frac{-0.060}{0.697}\right) = -0.1925$$

$$\frac{a_{21}}{a_{00}} = \sqrt{\frac{5\times 2}{3!}}\left(\frac{-0.040}{0.697}\right) = -0.0741 \tag{27}$$

$$\frac{b_{21}}{a_{00}} = \sqrt{\frac{5}{3}}\left(\frac{-0.051}{0.697}\right) = -0.0945.$$

This model in which the ice is assumed to be contained in a single circular ice cap and the oceans are geographically realistic may be simply extended to the case in which the oceans are fed by N circular ice caps of arbitrary radii α_i and colatitude-east longitude locations (θ_i', ϕ_i'). The inertia perturbations which replace (26) are then simply obtained by summing over separate contributions of the form (26) as

$$I_{13}^{R} = \sum_{i=1}^{N} M_i a^2 \left[\tfrac{1}{6} \cos\alpha_i(1+\cos\alpha_i) P_2^1(\cos\theta_i') \cos\phi_i' - \frac{a_{21}}{5a_{00}} \right]$$

$$I_{23}^{R} = \sum_{i=1}^{N} M_i a^2 \left[\tfrac{1}{6} \cos\alpha_i(1+\cos\alpha_i) P_2^1(\cos\theta_i') \sin\phi_i' - \frac{b_{21}}{5a_{00}} \right] \tag{28}$$

$$I_{33}^{R} = \sum_{i=1}^{N} M_i a^2 \left[\tfrac{2}{15} \frac{a_{20}}{a_{00}} - \tfrac{1}{3} \cos\alpha_i(1+\cos\alpha_i) P_2^0(\cos\vartheta_i') \right]$$

in which $P_2^1(\cos\theta) = -3\cos\theta\sin\theta$ and $P_2^0(\cos\theta) = (3\cos^2\theta - 1)/2$. The model embodied in (28) is the one we will use for most of the analyses to be described in the present paper. It is clearly considerably more accurate than the case (ii) model employed previously in SP. In order to facilitate comparison of our results with those obtained previously we will define a loading function L_n as

$$L_n = a^2 \iint \sigma(\vartheta, \phi) P_n^0(\cos\theta)\, ds$$

$$= \frac{4\pi a^2}{(2n+1)} \sigma_{n01} \tag{29}$$

so that from (13)

$$I_{33}^{R} = -\tfrac{2}{3} a^2 L_2 \tag{30}$$

since $\sigma_{001} \equiv 0$.

2.2 PERTURBATION OF INERTIA DUE TO ISOSTATIC ADJUSTMENT OF THE EARTH

In addition to the perturbations of inertia due to the direct effect of the surface mass load discussed in the last subsection, additional modifications of the inertia tensor are effected by the deformation of the Earth which these loads cause. The process by which this deformation takes place is called isostatic adjustment. For a homogeneous earth model it was shown in SP that the additional inertia perturbations could be computed as

$$I_{ij}^{D} = k_2^{L} * I_{ij}^{R} \tag{31}$$

in which I_{ij}^{D} are the inertia perturbations produced by the deformation of the Earth, k_2^{L} is the surface load Love number of degree 2, and the * denotes convolution in time. The physical meaning of k_2^{L} can be seen in the fact that when it is multiplied by the potential perturbation due to the load, it gives the perturbation of the gravitational potential at the Earth's surface due to the internal redistribution of mass produced by the deformation. All of the viscoelastic structure of the real Earth is embedded in this parameter.

In SP the result (31) was obtained for the special case of the homogeneous earth model by directly integrating the defining equation for I_{ij}. This is of the same form as (9). We simply expanded $x_i = x_i + u_i$ and $\rho = \rho_0 + \rho'$ and evaluated the linearized form of the integral using the expressions for the interior displacements u_i for the homogeneous model provided in Wu & Peltier (1982). This is a clumsy procedure and clearly does not suffice to demonstrate that the form (31) continues to hold for arbitrary viscoelastic stratification. A simple proof of the generality of (31) may be constructed using Green's identity but this will not be recorded here. We will simply state that the result holds for arbitrary linearly viscoelastic and radially stratified earth models. The total perturbation of inertia due to the direct effect of the load and the load-induced deformation is then:

$$\begin{aligned} I_{ij} &= I_{ij}^{R} + I_{ij}^{D} \\ &= (1 + k_2^{L}) * I_{ij}^{R} \end{aligned} \tag{32}$$

where the * denotes convolution in time and I_{ij}^{R} is defined in the last subsection.

2.3 PERTURBATIONS OF INERTIA DUE TO THE ROTATION-INDUCED DEFORMATION

The contribution to the inertia perturbations of the deformation associated with the variable rotation has been discussed in detail in Munk & MacDonald (1960) and Lambeck (1980). We will therefore provide only a cursory discussion of the form this contribution takes in the present subsection. The potential associated with the centrifugal force is

$$\psi = \tfrac{1}{2}\left[\omega^2 r^2 - (\omega_i x_i)^2\right] \tag{33}$$

which may be split into two terms as

$$\psi = \tfrac{1}{3}\,\omega^2 r^2 + \chi \tag{34}$$

in which χ may be expanded as

$$\chi = \frac{GM}{r}\left(\frac{a}{r}\right)^3 \sum_n \sum_m \left(C_{2m}\cos m\phi + S_{2m}\sin m\phi\right) P_n^m(\cos\theta) \tag{35}$$

with

$$C_{20} = \frac{a^3}{6GM}(\omega_1^2 + \omega_2^2 - 2\omega_3^2) * k_2^{\mathrm{T}}$$

$$C_{21} = -\frac{a^3}{3GM}\omega_1\omega_3 * k_2^{\mathrm{T}}$$

$$C_{22} = \frac{a^3}{12GM}(\omega_2^2 - \omega_1^2) * k_2^{\mathrm{T}} \tag{36}$$

$$S_{21} = -\frac{a^3}{3GM}\omega_2\omega_3 * k_2^{\mathrm{T}}$$

$$S_{22} = -\frac{a^3}{6GM}\omega_1\omega_2 * k_2^{\mathrm{T}}$$

in which k_2^{T} is the tidal Love number of degree 2. By employing MacCullagh's formula (e.g. Munk & MacDonald 1960; SP) we may derive expressions for the inertia perturbations associated with the changing rotation as

$$I_{13}^{\mathrm{Rot}} = \frac{k_2^{\mathrm{T}} * a^5 \omega_1\omega_3}{3G} \simeq \frac{k_2^{\mathrm{T}}}{k_{\mathrm{f}}} * m_1(C - A)$$

$$I_{23}^{\mathrm{Rot}} = \frac{k_2^{\mathrm{T}} * a^5 \omega_2\omega_3}{3G} \simeq \frac{k_2^{\mathrm{T}} *}{k_{\mathrm{f}}} m_2(C - A) \tag{37}$$

where

$$k_{\mathrm{f}} = \frac{3G}{a^5\Omega^2}(C - A) \tag{38}$$

is the so-called fluid Love number.

2.4 SOLUTION OF LIOUVILLE'S EQUATIONS IN THE LAPLACE TRANSFORM DOMAIN

In the previous subsections we have suppressed the explicit appearance of the time variation of the load. Since the precise form of the time history is in fact an important ingredient in the solution we require a way of introducing it into the previous theory. To do this we define the history function $f(t)$ such that

$$M(t) = Mf(t) \tag{39}$$

where f is a function which varies between 0 and 1. During an interglacial period $f \equiv 0$ while at absolute glacial maximum $f = 1$. The parameters $\sigma_{nmi}(t)$, $L_n(t)$ and $I_{ij}^{\mathrm{R}}(t)$ also have the same form as (39).

The analysis of subsection 2.3 established that the inertia perturbations produced by the response to the changing rotation depended linearly upon the m_i (equations 37). This makes it advantageous in (4) to separate the rotational and loading excitations as (Munk & MacDonald 1960)

$$\boldsymbol{\psi} = \boldsymbol{\psi}^{\mathrm{L}} + \boldsymbol{\psi}^{\mathrm{Rot}} \tag{40}$$

with

$$\psi_1^{\mathrm{Rot}} = \frac{k_2^{\mathrm{T}}}{k_{\mathrm{f}}} * \left(m_1 + \frac{\dot{m}_2}{\Omega}\right) \simeq \frac{k_2^{\mathrm{T}}}{k_{\mathrm{f}}} * m_1$$

$$\psi_2^{\mathrm{Rot}} = \frac{k_2^{\mathrm{T}}}{k_{\mathrm{f}}} * \left(m_2 - \frac{\dot{m}_1}{\Omega}\right) \simeq \frac{k_2^{\mathrm{T}}}{k_{\mathrm{f}}} * m_2. \tag{41}$$

Substitution of (40) and (41) into (4) and (5) followed by transformation to the domain of the Laplace transform variable s gives

$$\mathbf{m}(s) = \frac{-i\sigma_{\mathrm{r}}\psi^{\mathrm{L}}(s)}{[\![s - i\sigma_{\mathrm{r}}[1 - k_2^{\mathrm{T}}(s)/k_{\mathrm{f}}]]\!]} \tag{42}$$

$$m_3(s) = -\frac{I_{33}(s)}{C} \tag{43}$$

in which $\psi^{\mathrm{L}} = \psi_1^{\mathrm{L}} + i\psi_2^{\mathrm{L}}$ and from (8)

$$\psi_1^{\mathrm{L}}(s) = \frac{I_{13}(s)}{(C-A)} + \frac{[sI_{23}(s) - I_{23}(t=0)]}{\Omega(C-A)}$$

$$\psi_2^{\mathrm{L}}(s) = \frac{I_{23}(s)}{(C-A)} - \frac{[sI_{13}(s) - I_{13}(t=0)]}{\Omega(C-A)}. \tag{44}$$

If we assume that the system is unperturbed for $t \leqslant 0$ we may set $I_{13}(t=0) = I_{23}(t=0) = 0$. Also from the results of subsection 2.2 we have

$$I_{ij}(s) = [1 + k_2^{\mathrm{L}}(s)]\, f(s)\, I_{ij}^{\mathrm{R}} \tag{45}$$

so that

$$\psi^{\mathrm{L}}(s) = [\,1 + k_2^{\mathrm{L}}(s)]\, f(s)[(\psi_{13}^{\mathrm{R}} + i\psi_{23}^{\mathrm{R}}) + \frac{s}{\Omega}(\psi_{23}^{\mathrm{R}} - i\psi_{13}^{\mathrm{R}})\,] \tag{46a}$$

$$I_{33}(s) = [1 + k_2^{\mathrm{L}}(s)]\, f(s)\, I_{33}^{\mathrm{R}} \tag{46b}$$

in which

$$\psi_{13}^{\mathrm{R}} = \frac{I_{13}^{\mathrm{R}}}{(C-A)} = \frac{\Omega}{A\sigma_{\mathrm{r}}} I_{13}^{\mathrm{R}}$$

$$\psi_{23}^{\mathrm{R}} = \frac{I_{23}^{\mathrm{R}}}{(C-A)} = \frac{\Omega}{A\sigma_{\mathrm{r}}} I_{23}^{\mathrm{R}}. \tag{47}$$

Equations (42), (43) and (46), (47) are now complete and may be employed to model the processes in which we are interested. These equations are quite general since they assume nothing about the earth model other than that it is linearly viscoelastic and radially stratified, and nothing about the geometry of the load. We will now proceed to solve them subject to specific assumptions concerning these two functionals of the model. Analysis of the forced polar motion follows in Section 3 while the non-tidal acceleration is discussed in Section 4.

3 Deglaciation forced wander of the rotation pole

Given an appropriate stratified viscoelastic model of the planet we may calculate $k_2^{\mathrm{L}}(t)$ and $k_2^{\mathrm{T}}(t)$ using the methods developed in Peltier (1974, 1976). Given an appropriate spatial geometry and temporal history of glacial loading the functions I_{ij}^{R} and $f(t)$ are also known

and we may proceed to solve the model equations. In this section we will focus upon the decoupled equations (42) and (46a) which together determine the wander of the rotation pole relative to the surface geography which is produced by ice sheet accumulation and ablation. We will first solve this system (subsection 3.1) under the assumption that the earth model is homogeneous. This will allow us to explore the problems raised by the previously published analyses of this case contained in SP and NL. As we will show, it is impossible to fit the observed polar wander evident in the ILS pole path when a homogeneous earth model is employed along with a realistic loading history $f(t)$. Both of the previous analyses of this datum are therefore incorrect. In subsection 3.2 we investigate the question of whether a realistic stratified viscoelastic model might contain the necessary ingredients to allow us to fit the observed polar wander speed when the loading history is also realistic. As we will see, we shall be able to answer this question in the affirmative.

3.1 POLAR WANDER FOR A HOMOGENEOUS VISCOELASTIC EARTH MODEL

For a homogeneous viscoelastic sphere the Laplace transform domain expressions for k_2^{T} and k_2^{L} are (e.g. Munk & MacDonald 1960; Wu & Peltier 1982)

$$k_2^{\mathrm{T}}(s) = \frac{3/2}{1+\bar{\mu}} \left(1 + \frac{\gamma\bar{\mu}}{s+\gamma}\right) \tag{48a}$$

$$k_2^{\mathrm{L}}(s) = \frac{-1}{(1+\bar{\mu})} \left(1 + \frac{\gamma\bar{\mu}}{s+\gamma}\right), \tag{48b}$$

in which $\gamma = (\mu/\nu)/(1+\bar{\mu})$ is the inverse relaxation time of the degree two harmonic, μ the rigidity, and $\bar{\mu} = 19\mu/2\rho g a$ the non-dimensional rigidity of the earth model of radius a and density ρ, and surface gravitational acceleration g. In order that they might better mimic the Love numbers for the real Earth, both (48a) and (48b) must be modified slightly (Munk & MacDonald 1960). In practice we replace the factor 3/2 by k_{f} given in (38) such that k_2^{T} matches the observed flattening of the Earth in the static ($s \to 0$) limit. We similarly modify $k_2^{\mathrm{L}}(s)$ such that $1 + k_2^{\mathrm{L}}(0) = l_{\mathrm{s}} \neq 0$ which mimics the effect of the lithosphere in inhibiting the complete relaxation of the Earth in response to a surface load. These two modifications given k_2^{T} and k_2^{L} as

$$k_2^{\mathrm{T}}(s) = \frac{k_f}{1+\bar{\mu}} \left(1 + \frac{\gamma\bar{\mu}}{s+\gamma}\right) \tag{49a}$$

$$k_2^{\mathrm{L}}(s) = -\frac{(1-l_{\mathrm{s}})}{(1+\bar{\mu})} \left(1 + \frac{\gamma\bar{\mu}}{s+\gamma}\right) \tag{49b}$$

which are identical to the expressions employed in SP and in NL.

Initially at least we will assume that the viscoelastic earth model with Love numbers (49) is loaded by a single circular ice cap and a complementary ocean as described under case (ii) of 2.1. If the centre of the ice cap is at colatitude θ' and east longitude $\phi' = 0$ then combining (19) and (13) we obtain

$$I_{13}^{\mathrm{R}} = -\frac{a^2}{3} M \cos\alpha \sin\theta \cos\theta \tag{50a}$$

$$I_{23}^{\mathrm{R}} = 0 \tag{50b}$$

so that the definition of the excitation function in (46a) gives

$$\psi^{\mathrm{L}}(s) = -\frac{\Omega}{A\sigma_{\mathrm{r}}} [1 + k_2^{\mathrm{L}}(s)] f(s) \left(1 - \frac{is}{\Omega}\right) I_{13}^{\mathrm{R}}. \tag{51}$$

Substitution of this result into (42) gives a Laplace transform domain solution for the polar wander as

$$\mathbf{m} = -\frac{i\Omega}{A(\gamma - i\sigma_0)}\left[\frac{\gamma}{s} - \frac{i\sigma_0}{s+\gamma-i\sigma_0}\right][1+k_2^{\mathrm{L}}(s)]\left(1-\frac{is}{\Omega}\right)f(s)\,I_{13}^{\mathrm{R}} \tag{52}$$

in which $\sigma_0 = \sigma_r\bar{\mu}/(1+\bar{\mu})$ is the Chandler wobble frequency of the homogeneous deformable earth model. Note also that $(\gamma - i\sigma_0)^{-1}[\gamma/s - i\sigma_0/(s+\gamma-i\sigma_0)] = (s+\gamma-i\sigma_0)^{-1}[\gamma/s+1]$.

In order to understand clearly the differences between the approximate solutions of (52) obtained by SP and NL we will first obtain the exact time domain form of $\mathbf{m}$ by direct Laplace inversion. The detailed algebra will not be produced here since it is straightforward. The solution is such that the real part of $\mathbf{m}$, m_1, has the exact time domain form

$$m_1(t) = \frac{\Omega I_{13}^{\mathrm{R}}/(A\sigma_0)}{[1+(\gamma^2/\sigma_0^2)]}\left[\left[\gamma l_s\int_0^t f(t')\,dt' - \left(1+\frac{\gamma^2}{\sigma_0^2}\right)\left[l_s+\frac{\sigma_0}{\sigma_r}(1-l_s)\right]\frac{\sigma_0}{\Omega}f(t)\right.\right.$$
$$\left.\left. + C_1[f*\exp(-\gamma t)\sin\sigma_0 t] + C_2[f*\exp(-\gamma t)\cos\sigma_0 t]\right]\right] \tag{53a}$$

in which C_1 and C_2 are constants. The speed of polar wander may be obtained by direct time differentiation of (53a) as

$$\dot{m}_1(t) = \frac{\Omega I_{13}^{\mathrm{R}}}{A\sigma_0[1+(\gamma^2/\sigma_0^2)]}\left[\left[\gamma l_s f(t) - \left(1+\frac{\gamma^2}{\sigma_0^2}\right)\left[l_s+\frac{\sigma_0}{\sigma_r}(1-l_s)\right]\frac{\sigma_0}{\Omega}\dot{f}(t)\right.\right.$$
$$\left.\left. + C_1\frac{d}{dt}[f*\exp(-\gamma t)\sin\sigma_0 t] + C_2\frac{d}{dt}[f*\exp(-\gamma t)\cos\sigma_0 t]\right]\right] \tag{53b}$$

Both (53a) and (53b) are exact solutions to (52). Since the viscous decay time γ^{-1} is much greater than either the Chandler wobble period $2\pi/\sigma_0$, or the length of day $2\pi/\Omega$, we may safely make the approximations $\gamma/\Omega \simeq 0$, and $1 \pm \gamma^2/\sigma_0^2 \simeq 1$ to reduce (53b) to the form

$$\dot{m}_1(t) = \frac{\Omega}{A\sigma_0}\left[\left[\gamma(1+\bar{\mu})P_1 f(t) - \frac{\sigma_0}{\Omega}(P_1+P_2)\dot{f}(t)\right.\right.$$
$$+\frac{d}{dt}[f*\exp(-\gamma t)\sin\sigma_0 t]\left[\sigma_0\left(1+\frac{\sigma_0}{\Omega}\right)(P_1+P_2)\right]$$
$$\left.\left.+\frac{d}{dt}[f*\exp(-\gamma t)\cos\sigma_0 t]\left[-\gamma l_s + \frac{\gamma\sigma_0^2}{\Omega\sigma_r}(1-l_s)P_2\right]\right]\right] \tag{54}$$

where we have introduced

$$I_{13}^{\mathrm{R}} = \frac{\sigma_r}{\sigma_0}\frac{\bar{\mu}}{l_s}P_1 = \frac{\sigma_r}{\sigma_0}P_2$$

in order to make our results directly comparable with SP.

Now the expression for the polar wander speed in (54) contains both non-oscillatory terms and terms involving exponentially damped sinusoidal oscillations at the Chandler frequency σ_0 and having decay constant γ^{-1}. In order to reveal the secular part of the solution clearly we simply apply a running average over the Chandler period to equation (54). This procedure eliminates the last two terms with the exception of a contribution in the amount $f(t)(1+\sigma_0/\Omega)(P_1+P_2)$ from the second-last term. If we denote these filtered

solutions with a bar then

$$\bar{m}_1(t) = \frac{\Omega}{A\sigma_0}\left[\gamma(1+\bar{\mu})\,P_1\int_0^t f(t')\,dt' + (P_1+P_2)\,f(t)\right] \tag{55a}$$

$$\dot{\bar{m}}(t) = \frac{\Omega}{A\sigma_0}\left[\gamma(1+\bar{\mu})\,P_1 f(t) + (P_1+P_2)\,\dot{f}(t)\right]. \tag{55b}$$

It is equation (55b) which is to be employed to fit the observed $0.95°/10^6$yr drift speed revealed by the ILS data shown in Fig. 1. A much more straightforward way of arriving at the low-frequency solution (55) is simply to note from (52) that in the limit

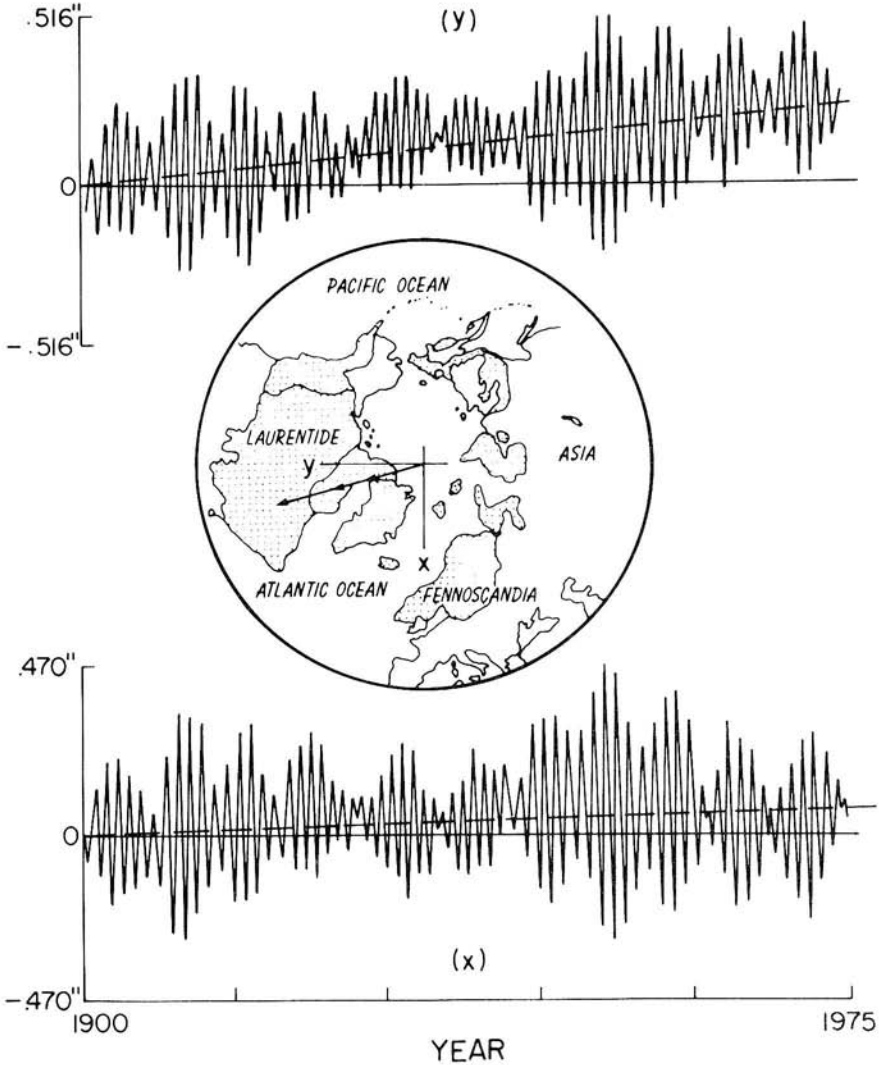

Figure 1. ILS data showing the location of the rotation pole relative to the CIO (conventional international origin) as a function of time since AD 1900. The 7 yr beat in the polar motion signal is a consequence of the superposition of the 12 month forced annual wobble and the 14 month Chandler wobble. This oscillatory signal is superimposed upon the slow secular drift denoted by the dashed lines which corresponds to a polar wander speed of approximately $0.95°/10^6$ yr. This secular drift is the signal of interest in the present paper.

$s/\sigma_0 \ll 1$ the second term in square brackets on the right-hand side tends to unity (since $\gamma \ll \sigma_0$). Subject to this approximation, and using $\gamma \leq \sigma_0$, Laplace transformation yields (55) directly.

The result (55) is radically different from the solution for the homogeneous earth model published previously in SP. There the assumption was made that the second term in square brackets in (52) could be neglected compared to the first. Although this does remove the Chandler wobble it also eliminates a crucial contribution to the low-frequency (secular) wander of the pole. Subject to this invalid approximiation, the result which replaces (55) is

$$\dot{\bar{m}}_1^{\mathrm{SP}}(t) = \frac{\Omega}{A\sigma_0}\left[\left[\gamma(1+\bar{\mu})\,P_1 f(t) + \gamma(P_2 - \bar{\mu}P_1)\frac{d}{dt}[f * \exp(-\gamma t)]\right]\right] \tag{56}$$

which differs from (55) in that it contains a term involving the convolution of the glaciation history $f(t)$ with the decaying exponential $\exp(-\gamma t)$. This term clearly introduces a history dependence into the SP solution which does not exist in the correct solution for the homogeneous model given in (55). It might be naively expected that the correct solution *should* possess a history dependence of the sort which appears in (56). After all, as we have heard the argument expressed, the relaxation of the Earth continues long after the time at which the surface load has ceased to vary: this should be accompanied by a variation of the inertia tensor and therefore by a forced polar motion. This naive expectation is completely unfounded. For the homogeneous model, but only for the homogeneous model, the forcing associated with the free relaxation of the Earth's shape is exactly cancelled by the forcing associated with the rotational deformation. The rotational deformation amplifies the moment of inertia with respect to the z-axis while isostatic adjustment of the load diminishes it. Since these two opposing effects have the same relaxation time constant, they can (and do) cancel each other at all times (also see Munk & MacDonald 1960, section 6.4, who discuss precisely this point) and the instantaneous rotational response to the changing surface load has no memory of earlier states of the system.

Give this physical understanding of the solution (55) for the homogeneous earth model we will proceed to discuss the previous attempts by SP and by NL to use this model to interpret the data shown on Fig. 1. The analyses in these papers differ in two important ways and each contains an error which it will be important for us to understand. NL obtain the correct form of the solution (55) for the homogeneous earth model. However, they assume a loading history which is unrealistic in that an *exact* state of isostatic equilibrium is assumed to exist prior to the time melting commences. The deglaciation event is assumed to be uniform over a period of about 10 kyr as depicted on the insert of Fig. 2(a). At the end of the deglaciation period the loaded regions are therefore assumed to be subjected to a net negative load which remains constant after deglaciation is complete. Using the numerical values of the parameters given in Table 1 the $\dot{\bar{m}}_1(t)$ prediction for this loading history is shown in Fig. 2(a). Following the deglaciation period the predicted speed of polar wander is positive (polar motion towards the unloaded region) and constant. In Fig. 2(a) we show $\dot{\bar{m}}_1(t)$ for two different viscosity models, one with $\nu = 10^{22}$ P (dashed line) and one with $\nu = 3 \times 10^{21}$ P (solid line). $\dot{\bar{m}}_1$ is always positive because the rotation pole always tends to align itself with the axis of greatest inertia and this passes through the centre of deglaciation. Following deglaciation, $\dot{\bar{m}}_1$ is determined from (73) to be

$$\begin{aligned}\dot{\bar{m}}_1(t) &= \frac{\Omega}{A\sigma_0} \cdot \gamma(1+\bar{\mu})\,P_1 f(t) \\ &= \frac{\Omega(1+\bar{\mu})}{A\sigma_r\bar{\mu}} \cdot I_{13}^{\mathrm{R}} \cdot f(t) \cdot (l_s \cdot \gamma).\end{aligned} \tag{57}$$

The dependence upon the viscosity ν enters through $\gamma = (\mu/\nu)/(1+\tilde{\mu})$. Equally crucial however is the 'isostatic factor' l_s defined previously as

$$l_s = \lim_{s \to 0} [1 + k_2^L(s)]. \tag{58}$$

As shown in detail in Wu & Peltier (1982) the value of the isostatic factor is principally controlled by the thickness of the lithosphere. In constructing Fig. 2(a) we fixed the lithosphere thickness L to have the same value as that assumed by NL, i.e. $L = 120$ km. To

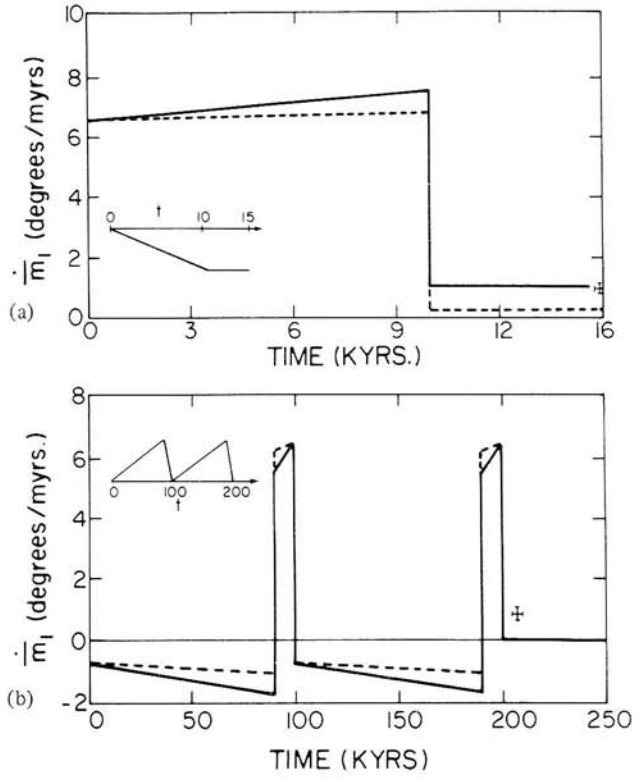

Figure 2. The upper plate (a) shows the prediction of polar wander speed for a homogeneous viscoelastic earth model subject to the deglaciation event shown in the inset which is such that isostatic equilibrium is assumed to obtain initially. Subject to this assumption the model can fit the data which are shown as the cross near the right hand margin of the figure. The lower plate (b) shows the prediction of polar wander speed for a homogeneous viscoelastic earth model subject to the periodic glaciation history shown on the inset. The observed $0.95°/10^6$ yr drift speed obtained from the data of Fig. 1 is again shown as the cross. This model cannot fit the data since it predicts a drift speed which is identically zero whenever the system is neither glaciating nor deglaciating – as is the case today.

Table 1. Earth model parameters.

Mean radius a	6.371×10^6 m
Mass M_e	5.976×10^{24} kg
Surface acceleration	9.82 m s^{-2}
Principal moments of inertia	
C	0.8019×10^{38} kg m^2
A	0.7992×10^{38} kg m^2
Rate of angular rotation Ω	2.3012×10^5 rad kyr^{-1}
Chandler frequency (rigid) σ_r	0.7676×10^4 rad kyr^{-1}
Average elastic shear modulus μ	1.4519×10^{11} N m^{-2}

fit the observed $0.95°/10^6$ yr drift speed indicated by the data in Fig. 1, shown as the cross in Fig. 2(a), would clearly require a viscosity near 3×10^{21} P for the mantle. The analyses in NL suggest a value nearer 8×10^{21} P and the difference between our result and theirs may be understood simply as a consequence of the fact that they have employed a considerably more elaborate loading history (based upon the ICE-1 history tabulated in Peltier & Andrews 1976).

The assumption that the initial state was one of exact isostatic equilibrium, upon which the NL calculation was based, is incorrect, however, and before we can have any confidence in the result for the mantle viscosity we should test the stability of the inference against the introduction of a more reasonable glaciation history. There does in fact exist a rather useful set of data which can be invoked to constrain the glaciation history strongly throughout the 2×10^6 yr period of the Pleistocene. This consists of oxygen isotope data from sedimentary cores taken in the deep ocean basins. An example of the $^{18}O/^{16}O$ ratio as a function of depth from one such core is shown in Fig. 3 where it is compared to a simple sawtooth function with a period of 10^5 yr. It is generally accepted, following the work of Shackleton (1967) and Shackleton & Opdyke (1973), that this isotopic ratio is directly dependent upon the volume of ice bound in continental complexes. Equally apparent by inspection of Fig. 3 and on the basis of spectral analyses of such isotopic time series (e.g. see Hays, Imbrie & Shackleton 1976) is the fact that the variance in the ice coverage fluctuations is dominated by an almost periodic fluctuation with period 10^5 yr. Peltier (1982) provides a theory for the existence of this periodic fluctuation but this topic is outside the scope of the present paper. The detailed analysis of the shape of the ice volume fluctuation between successive interglacials has recently been discussed by Kukla *et al.* (1981) who demonstrate that the dominant 10^5 yr fluctuation is characterized by a gradual build-up of the ice mass over a period of about 9×10^4 yr followed by a more rapid retreat over a period of about 10^4 yr. Thus justifies as a first approximation our representation of the glaciation history by the sawtooth wavefunction shown in Fig. 3.

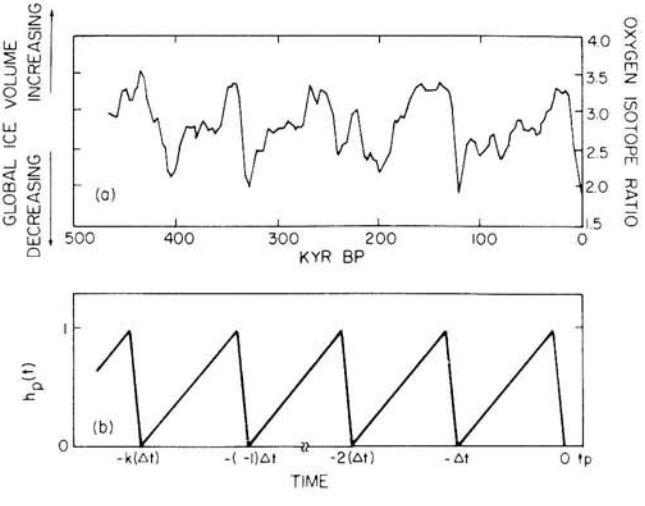

Figure 3. The upper plate shows a typical $^{18}O/^{16}O$ time series from a deep sea sedimentary core. Such series provide strong control upon the Pleistocene history of continental ice volume fluctuations. The lower plate shows a sawtooth approximation to the loading history implied by the oxygen isotopic data. The dominant period of the ice volume record is near 10^5 yr and each cycle is characterized by a slow build-up of ice followed by a rapid retreat.

This new loading history, which provides a much more realistic representation of the actual load cycle than that assumed in NL, is also illustrated in the inset to Fig. 2(b). When this load history is inserted into equation (55), we obtain the $\dot{\bar{m}}_1(t)$ shown in Fig. 2(b). In constructing this figure we have assumed two cycles of loading but it is quite clear from the absence of any history-dependent term in (55) that the number of cycles has no influence at all on the predicted results. Since the load is assumed to be zero following the second cycle the model predicts an observed polar wander speed which is identically zero also. Since we are at present living at such a time of apparent hiatus in a previously continuous Pleistocene glacial cycle, the observed non-zero polar wander speed (shown as the cross) cannot be fitted by the homogeneous model. If the load cycle were not interrupted it is clear that the misfit would only be increased. This result is of course independent of the mantle viscosity, results for two values of which are shown as the solid and dashed curves in Fig. 2(b). It is therefore clear that the polar wander analysis of NL is inappropriate because the homogeneous model which they employ cannot fit the data, no matter what values are chosen for the model parameters, when a realistic load cycle is assumed. What of the parallel analysis using the homogeneous model by SP?

The analysis of SP was based upon the erroneous solution (56) which was constructed on the basis of the incorrect assumption that the second term in square brackets on the rhs of (52) could be completely neglected. Because (56) contains a history-dependent term, even when a realistic load cycle is assumed (as in SP) it will not predict a zero polar wander speed when the load cycle is interrupted. It is due to the presence of this history-dependent term in their solution that SP were able to fit the homogeneous model subject to cyclic loading, to the polar wander observed in Fig. 1. This erroneous analysis also led SP to claim that this datum required a mantle viscosity near 10^{22} P.

We are therefore at something of an impasse since it has been shown to be impossible to fit the rate and direction of drift revealed in the ILS pole path with a homogeneous viscoelastic earth model subject to cyclic glaciation and deglaciation. The only possible way out of this dilemma is that when the radial stratification of the real viscoelastic Earth is taken into account we will again be able to fit the observation. This hope turns out to be justified as we demonstrate in the following subsection.

3.2 POLAR WANDER FOR A STRATIFIED VISCOELASTIC EARTH MODEL

As demonstrated in Peltier (1976), the main difference between homogeneous and stratified viscoelastic earth models is that the viscous component of the response in the former case is carried by a single normal mode of viscous gravitational relaxation (see also Wu & Peltier 1982). In the stratified case, however, there are several distinct modes of relaxation which are required to describe the adjustment process. The analysis in the previous subsection shows that in the one-mode case the rotational excitation and isostatic adjustment excitation precisely cancel one another when the forcing vanishes. In this subsection we will show that this is not the case for the stratified model which supports a spectrum of viscously decaying modes. If there are N modes in the spectrum then the tidal and load Love numbers of degree 2 may be written (Peltier 1976) as

$$k_2^{\mathrm{T}}(s) = k_2^{\mathrm{TE}} + \sum_{j=1}^{N} \frac{t_j}{s + s_j} \tag{59a}$$

$$k_2^{\mathrm{L}}(s) = k_2^{\mathrm{LE}} + \sum_{j=1}^{N} \frac{r_j}{s + s_j} \tag{59b}$$

which have the following time domain forms

$$k_2^{\mathrm{T}}(t) = k^{\mathrm{TE}}\delta(t) + \sum_{j=1}^{N} t_j \exp(-s_j t) \tag{60a}$$

$$k_2^{\mathrm{L}}(t) = k^{\mathrm{LE}}\delta(t) + \sum_{j=1}^{N} r_j \exp(-s_j t). \tag{60b}$$

For comparison with our previous analyses it will prove useful to define $k_2^{\mathrm{T}}(0) = k_2^{\mathrm{T}}(s=0)$ and $l_s = 1 + k_2^{\mathrm{L}}(0)$. Equations (59) may then be rewritten

$$k_2^{\mathrm{T}}(s) = k_2^{\mathrm{T}}(0) - s\sum_{j=1}^{N} \frac{(t_j/s_j)}{(s+s_j)} \tag{61a}$$

$$k_2^{\mathrm{L}}(s) = (-1 + l_s) - s\sum_{j=1}^{N} \frac{(r_j/s_j)}{(s+s_j)}. \tag{61b}$$

We will also define

$$\sigma_0 = \frac{(k_2^{\mathrm{T}}(\mathrm{o}) - k_2^{\mathrm{TE}})}{k_2^{\mathrm{T}}(\mathrm{o})}\,\sigma_{\mathrm{r}} \tag{62}$$

to be the Chandler wobble frequency of the deformable stratified earth and will introduce the parameter ϵ (second-order quantity)

$$\epsilon = 1 - \frac{k_2^{\mathrm{T}}(\mathrm{o})}{k_f} \simeq 0. \tag{63}$$

Equation (42) for the statified model then assumes the form

$$\mathbf{m}(s) = \frac{-i\sigma_{\mathrm{r}}\psi^{\mathrm{L}}(s)}{s\left[1 - \dfrac{i\sigma_{\mathrm{r}}}{k_{\mathrm{f}}}\displaystyle\sum_{j=1}^{N}\frac{t_j}{s_j(s+s_j)}\right]} \tag{64}$$

As shown in the last subsection we may remove the Chandler wobble terms from the frequency domain form of the solution without changing the secular component of the response by simply assuming $|s|/\sigma_0 \ll 1$. Also since $s_j \ll \sigma_{\mathrm{r}} < \Omega$, and since $t_j/(s_j k_{\mathrm{f}}) \lesssim O(1)$, thus $\sigma_{\mathrm{r}}\, t_j/(s+s_j)(s_j k_{\mathrm{f}}) \gg 1$. This means that the first term (unity) in square brackets in the denominator of (64) may be neglected. This approximation reduces (64) to the form

$$\mathbf{m}(s) = \frac{\psi^{\mathrm{L}}(s)}{\dfrac{s}{k_{\mathrm{f}}}\displaystyle\sum_{j=1}^{N}\frac{t_j}{s_j(s+s_j)}}. \tag{65}$$

The solution for the stratified case is completed using (46) and (47) which give

$$\psi^{\mathrm{L}}(s) = \frac{\Omega}{A\sigma_{\mathrm{r}}}\,[1 + k_2^{\mathrm{L}}(s)]\, f(s)(I_{13}^{\mathrm{R}} + iI_{23}^{\mathrm{R}}) \tag{66}$$

where I_{13}^{R} and I_{23}^{R} may be evaluated as discussed in subsection 2.1.

Our solution for the stratified model (65) may be compared with that given in Sabadini, Yuen & Boschi (1982a, b) for a simple stratified incompressible model similar in other respects to our own. Sabadini *et al.* (their equation 75) make the further approximation

that s may be neglected with respect to s_j in the denominator of (65). This approximation is entirely analogous to the neglect for the homogeneous model of the second term in brackets on the rhs of (52). It is therefore equally incorrect, as pointed out in Peltier (1982). Physically this approximation amounts to assuming that the adjustment to the tidal deformation is instantaneous, an assumption which is obviously wrong since both the isostatic and rotational responses are governed by the same set of viscoelastic decay times.

It will simplify the analysis at this point if we first define

$$g_j = \frac{t_j/s_j}{\sum_{i=1}^{N} (t_i/s_i)} \tag{67}$$

which has the physical interpretation of the relative strength of the jth mode. Using (62) and (63) we may also write

$$k_f = \frac{\sigma_r}{\sigma_0} \sum_{j=1}^{N} \frac{t_j}{s_j} \tag{68}$$

which may be employed to reduce (65) to the form

$$\mathbf{m}(s) = \frac{\sigma_r}{\sigma_0} \frac{\psi^L(s)}{s \sum_{j=1}^{N} \frac{g_j}{(s+s_j)}} \tag{69}$$

Substituting (66) in (69), and making use of (6) yields

$$\bar{m}_i(s) = \frac{\Omega}{A\sigma_0} I_{i3}^R \frac{[1+k_2^L(s)]\, f(s)}{s \sum_{j=1}^{N} g_j/(s+s_j)}. \tag{70}$$

This is the final form of the solution in the Laplace transform domain.

In order to express this solution in the time domain, it will clearly help to express the factor

$$\frac{[1+k_2^L(s)]}{s \sum_j g_j/(s+s_j)} \tag{71}$$

in the form of a simple polynomial in s. In order to do this we first expand

$$\sum_{j=1}^{N} \frac{g_j}{(s+s_j)} = \frac{Q_{N-1}(s)}{\prod_{i=1}^{N} (s+s_i)} \tag{72}$$

by bringing this function to a common denominator. $Q_{N-1}(s)$ is a polynomial in s of degree $N-1$ with roots $\lambda_1, \ldots, \lambda_{N-1}$ say, i.e.

$$Q_{N-1}(s) = \sum_j g_j [\prod_{i \neq j} (s+s_i)] = \prod_{i=1}^{N-1} (s+\lambda_i). \tag{73}$$

Using (61b) we may then rewrite (71) as

$$\frac{1+k_2^{\mathrm{L}}(s)}{s\sum_{j=1}^{N}\frac{g_j}{(s+s_j)}} = \left[\frac{(s+s_1)\ldots(s+s_N)}{(s+\lambda_1)\ldots(s+\lambda_{N-1})}\right]\left[\frac{l_s}{s}+\sum_{j=1}^{N}\frac{(-r_j/s_j)}{(s+s_j)}\right]$$

$$= \frac{(s+s_1)\ldots(s+s_N)}{s(s+\lambda_1)\ldots(s+\lambda_{N-1})}\,l_s + \sum_{j=1}^{N} -\left(\frac{r_j}{s_j}\right)\left[\frac{\prod_{i\neq j}(s+s_i)}{\prod_{i=1}^{N-1}(s+\lambda_i)}\right]. \tag{74}$$

Since the first term cannot be inverted as it stands because the numerator and denominator have the same degree, it must be rewritten as

$$\frac{(s+s_1)\ldots(s+s_N)}{[s(s+\lambda_1)\ldots(s+\lambda_{N-1})]} = 1 - \frac{q(s)}{s(s+\lambda_1)\ldots(s+\lambda_{N-1})} \tag{75}$$

where

$$q(s) = s\prod_{i=1}^{N-1}(s+\lambda_i) - \prod_{i=1}^{N}(s+s_i). \tag{76}$$

For the same reason we must rewrite the factor in the second term of (74) as

$$\prod_{i\neq j}(s+s_i)\Big/\prod_{i=1}^{N-1}(s+\lambda_i) = 1 - \frac{R_j(s)}{(s+\lambda_1)\ldots(s+\lambda_{N-1})} \tag{77}$$

where

$$R_j(s) = \prod_{i=1}^{N-1}(s+\lambda_i) - \prod_{i\neq j}(s+s_i). \tag{78}$$

Using standard tables of Laplace transforms we may now invert (70) into the time domain to obtain

$$\bar{m}_j(t) = \frac{\Omega}{A\sigma_0} I_{j3}^{\mathrm{R}}\left[D_1 f(t) + D_2\int_0^t f(t')\,dt' + \sum_{i=1}^{N-1} E_i(f * \exp(-\lambda_i t)\right] \tag{79}$$

in which

$$\begin{aligned} D_1 &= l_s - \sum_{j=1}^{N}\frac{r_j}{s_j} = 1 + k_2^{\mathrm{LE}} \\ D_2 &= -\frac{l_s q(0)}{\prod_{i=1}^{N-1}\lambda_i} \\ E_i &= \left[\frac{l_s q(-\lambda_i)}{\lambda_i} + \sum_{j=1}^{N}\frac{r_j R_j(-\lambda_i)}{s_j}\right]\Big/\prod_{k\neq i}^{N-1}(\lambda_k - \lambda_i). \end{aligned} \tag{80}$$

The components of the polar wander velocity may be obtained from (79) by direct time differentiation which gives

$$\dot{\bar{m}}_j = \frac{\Omega}{A\sigma_0} I_{j3}^{\mathrm{R}}\left[D_1\dot{f}(t) + D_2 f(t) + \prod_{i=1}^{N-1} E_i\frac{d}{dt}[f * \exp(-\lambda_i t)]\right]. \tag{81}$$

Equations (79), (80) and (81) provide the correct polar wander solution for an arbitrary compressible, radially stratified, Maxwell viscoelastic earth model. This solution is completely different from that obtained by Sabadini *et al.* (1982) and is one of the main results of this paper (see also Peltier 1982). We will proceed to provide a thorough explanation of the properties of this solution here, although even the most cursory examination will reveal the fundamental way in which it differs from that for the homogeneous model given in equation (55). Equation (81) clearly contains the history-dependent term which is required if the polar wander speed is not to drop to zero immediately after the glacial forcing f drops to zero. If the general solution did not contain such a term then we known, from our analysis in the last subsection, that it could not possibly fit the observation when a realistic cyclic loading history is included in the calculation.

In order to establish that the magnitude of the history term, for a realistic earth model and applied load, is such as to allow the stratified model to fit the observation in Fig. 1, we must perform explicit calculations. In Fig. 4 we show the results obtained from a preliminary analysis in which the glaciation history f consists of either one or two cycles of duration 10^5 yr as illustrated in the top plate. We have assumed a single circular ice cap of Laurentian scale and location whose parameters are listed in Table 2. The convolution integrals $f * \exp(-\lambda_i t)$ which are required in order to construct the general solution (99) are evaluated in the Appendix and the computed history of polar wander speed $\dot{m}_1(t)$ is shown

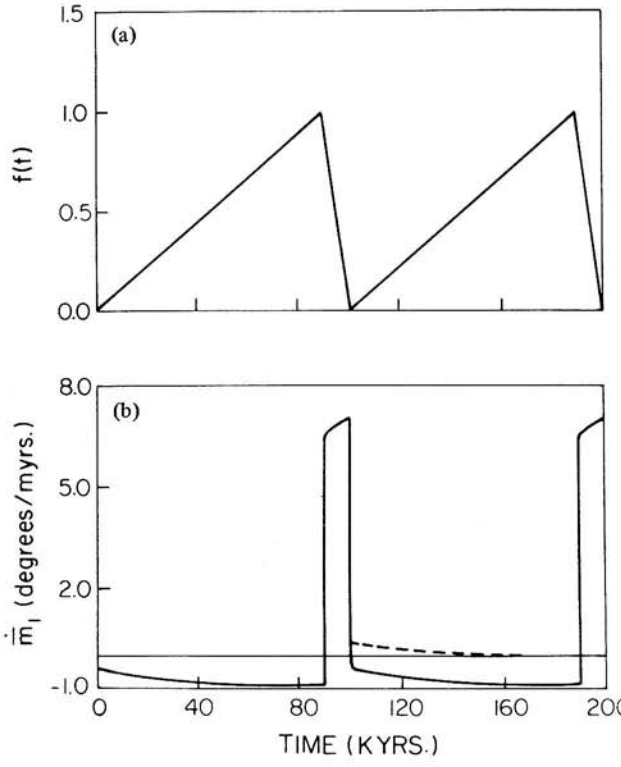

Figure 4. (a) The sawtooth approximation to the loading history. (b) The prediction of polar wander speed as a function of time for a stratified viscoelastic earth model subject to cyclic loading by a single circular ice cap. The dashed line shows the prediction of polar wander speed when the loading event ceases after the first cycle. In this case the speed does not drop immediately to zero as it did in Fig. 2 for the homogeneous model. It is this which allows the stratified model to fit the data when the homogeneous model cannot.

Table 2. Ice sheet parameters.

	Laurentian	Fennoscandian	Antarctic
Mass M_i (kg) ($\times 10^{19}$)	2	0.56	0.70
Radius α_i (°)	15	9.5	20
Colatitude θ_i (°)	30	25.5	180
East longitude ϕ_i (°)	270	25.0	–

Table 3. Inertia perturbations I^R_{i3} with realistic oceans and direction of polar wander θ.

	I^R_{13} (kg m^2)	I^R_{23} (kg m^2)	$I^R_{33}(\times 10^{32})$	θ
Laurentia only (L)	1.203×10^{31}	3.491×10^{32}	−3.420	−91.°97
Fennoscandia only (F)	-7.504×10^{31}	-3.227×10^{31}	−1.130	23.°27
Antarctica only (a)	4.211×10^{30}	5.370×10^{30}	−1.799	−128.°10
L + F	-6.301×10^{31}	3.168×10^{32}	−4.550	−78.°75
L + F + A	-5.880×10^{31}	3.222×10^{32}	−6.349	−79.°60

in the bottom plate for the case in which the load history consists of two cycles (solid curve) and the case in which loading ceases after a single cycle (dashed curve). Both calculations are for viscoelastic earth model L1 discussed in Wu & Peltier (1982) which has 1066B elastic structure (Gilbert & Dziewonski 1975), a lithospheric thickness of 120 km, and a constant mantle viscosity of 10^{21} Pa s. Inspection of Fig. 4 clearly shows that the effect of the history term is to prevent the polar wander speed from dropping to zero when the loading goes to zero (the dashed curve). It is furthermore clear that the magnitude of the speed is of about the right order to enable the model (with some adjustment of parameters) to come close to fitting the $\sim 0.95°/10^6$ yr speed implied by the data in Fig. 1. In order to make the fullest use of the observational datum, however, we will have to refine our calculation somewhat and explore the dependence of the theoretical prediction upon the parameters of the model.

In the remainder of this section (and of this paper) we will assume a coordinate system with x_1 directed along the Greenwich meridian and x_2 along the 90° east meridian (note that this is different from the coordinate system in Fig. 1 in that the direction of the x_2-axis is reversed). We will furthermore assume that the loading history includes three geographically separate centres of glaciation corresponding to the Laurentian, Fennoscandian and Antarctic ice masses. Detailed deglaciation histories for each of these three regions are tabulated in Wu & Peltier (1983). On the basis of these tabulations we have obtained the disc load approximations with parameters listed in Table 2. We will also assume that the geometry of the source of water which feeds these ice masses is realistic and thus described by the ocean function $\xi(\theta, \phi)$. Under these conditions the I^R_{i3} may be computed using equations (27) and (23), the results from which are listed in the first three columns of Table 3.

We have investigated the polar wander predictions of the general solution (81) for a wide range of compressible viscoelastic models including those which have the same 1066B elastic structure which fits a large quantity of seismic body wave and free oscillation data. Some of the calculations to be reported in this paper have been performed using incompressible multiple homogeneous layer approximations to the structure of 1066B although the compressibility of the lithosphere is always taken into account. Some of these simplified models are illustrated in Fig. 5 where they are numbered 1–3. These numbers denote the number of major density discontinuities in the structure. Thus model 1 has the density jump between the core and mantle, model 2 also includes the density change across the 670 km discontinuity, and model 3 has that across the 420 km discontinuity also. Also shown on the

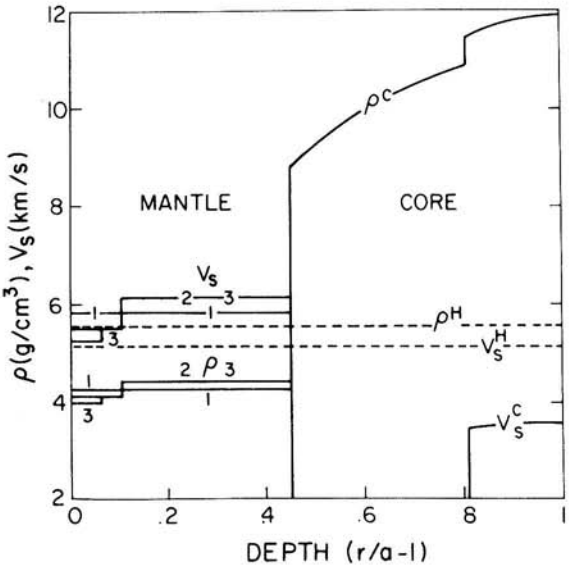

Figure 5. Elastic structures for some of the layered models discussed in the text. The number adjacent to each curve denotes the number of internal density discontinuities in the interior.

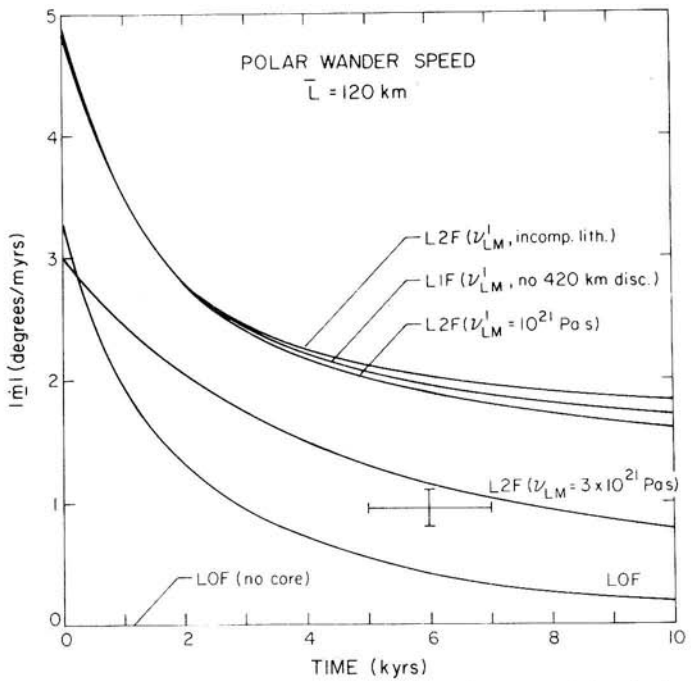

Figure 6. Predicted polar wander velocity as a function of time for some of the elastic models shown in Fig. 5. The zero of time is taken to be coincident with the end of the final deglaciation phase of a glaciation history consisting of 7 complete cycles. The polar wander speed implied by the data in Fig. 1 is shown as the cross at a time (t = 6 kyr) such as to provide a reasonable fit of the final deglaciation phase of the loading history of the ICE-2 chronology listed in Wu & Peltier (1983).

Table 4. Parameters for realistic earth models.

Parameters	Model A		Model B		Model C	
L, ν_{LM}	120.7 km	10^{21} Pa s	120.7 km	3×10^{21} Pa s	30 km	10^{21} Pa s
$D_1 D_2$	0.719	7.55×10^{-4}	0.719	7.06×10^{-4}	0.723	3.08×10^{-4}
s_1 (T4)	4.15 kyr^{-1}		3.82 kyr^{-1}		4.17 kyr^{-1}	
s_2 (T3)	3.95		3.71		3.95	
s_3 (T2)	3.58		3.34		3.61	
s_4 (T1)	3.48		3.09		3.49	
s_5 (M0)	1.92		7.19×10^{-1}		1.86	
s_6 (C0)	3.88×10^{-1}		1.79×10^{-1}		3.12×10^{-1}	
s_7 (L0)	9.79×10^{-2}		5.39×10^{-2}		2.54×10^{-2}	
s_8 (M1)	4.08×10^{-4}		2.90×10^{-4}		5.58×10^{-4}	
s_9 (M2)	9.01×10^{-6}		8.02×10^{-6}		1.35×10^{-5}	
r_1, t_1	-5.93×10^{-3}	8.77×10^{-3}	-9.32×10^{-3}	1.09×10^{-2}	-5.92×10^{-3}	9.49×10^{-3}
r_2, t_2	-1.25×10^{-2}	1.45×10^{-2}	-3.41×10^{-4}	6.16×10^{-4}	-1.31×10^{-2}	1.53×10^{-2}
r_3, t_3	-6.73×10^{-3}	9.35×10^{-3}	-1.02×10^{-2}	1.19×10^{-2}	-6.66×10^{-3}	9.79×10^{-3}
r_4, t_4	-1.45×10^{-2}	1.67×10^{-2}	-4.44×10^{-3}	7.36×10^{-3}	-1.66×10^{-2}	1.91×10^{-2}
r_5, t_5	-7.61×10^{-1}	9.35×10^{-1}	-2.77×10^{-1}	3.43×10^{-1}	-7.54×10^{-1}	9.41×10^{-1}
r_6, t_6	-8.16×10^{-2}	5.86×10^{-2}	-2.90×10^{-2}	2.25×10^{-2}	-8.75×10^{-2}	5.71×10^{-2}
r_7, t_7	-5.81×10^{-3}	2.82×10^{-3}	-6.71×10^{-3}	3.65×10^{-3}	-2.95×10^{-5}	4.35×10^{-5}
r_8, t_8	-8.37×10^{-6}	1.13×10^{-6}	-5.56×10^{-6}	7.12×10^{-7}	-1.13×10^{-5}	1.58×10^{-6}
r_9, t_9	-1.39×10^{-8}	8.62×10^{-10}	-9.70×10^{-9}	5.50×10^{-10}	-1.41×10^{-8}	8.23×10^{-10}
λ_1, E_1	4.15 kyr^{-1}	1.36×10^{-3}	3.80 kyr^{-1}	1.38×10^{-3}	4.16 kyr^{-1}	1.68×10^{-3}
λ_2, E_2	3.94	8.68×10^{-4}	3.71	2.71×10^{-4}	3.94	8.10×10^{-4}
λ_3, E_3	3.57	1.04×10^{-3}	3.33	1.39×10^{-3}	3.61	1.27×10^{-3}
λ_4, E_4	3.46	9.47×10^{-4}	3.08	2.73×10^{-3}	3.48	9.56×10^{-4}
λ_5, E_5	7.80×10^{-1}	1.57×10^{-1}	3.16×10^{-1}	5.29×10^{-2}	7.25×10^{-1}	1.71×10^{-1}
λ_6, E_6	1.32×10^{-1}	2.53×10^{-2}	8.64×10^{-2}	1.66×10^{-2}	2.75×10^{-2}	5.33×10^{-4}
λ_7, E_7	3.40×10^{-3}	2.52×10^{-2}	1.23×10^{-3}	8.18×10^{-3}	3.60×10^{-3}	1.57×10^{-2}
λ_8, E_8	2.09×10^{-5}	1.02×10^{-3}	1.40×10^{-5}	5.50×10^{-4}	2.33×10^{-5}	2.90×10^{-4}

Table 5. Effects of lithospheric thickness variations upon the model parameters.

L (km)	k_2^{TE}	k_2^{T} $(s=0)$	σ_0 (kyr^{-1}) $(\times10^4)$	k_2^{LE}	k_2^{L} $(s=0)$	l_s
0	0.29558	0.93081	0.524	−0.30495	−1.000	0
120.7	0.29558	0.91640	0.520	−0.30495	−0.99097	0.009
195.6	0.29558	0.90737	0.518	−0.30495	−0.98446	0.016
295.3	0.29558	0.89450	0.514	−0.30495	−0.97320	0.027

figure by the dashed lines are the parameters for the homogeneous model discussed previously. The viscosity structures of all models which we will consider are parameterized by three numbers $\bar{L}$, ν_{UM} and ν_{LM} which respectively denote the thickness of the lithosphere in which $\nu = \infty$ and the viscosities of the upper and lower mantles. Table 4 lists the data required in equation (81) for three different models which have the elastic structure denoted by the number 3 in Fig. 5. For each model ν_{UM} is fixed at 10^{21} Pa s and the models therefore differ only in their values of ν_{LM} and L. The data listed in Table 5 demonstrate the influence of lithospheric thickness upon the tidal and load Love number asymptotes, the Chandler frequency σ_0, and the isostatic factor l_s when the basic elastic structure is fixed to that of 1066B.

In Fig. 6 we have plotted the magnitude of the polar wander velocity vector $(\dot{m}_1, \dot{m}_2)$ as a function of time since the end of the last deglaciation event for a subset of the above described models. Prior to the zero of time, we have assumed the occurrence of seven cycles of glaciation and deglaciation, each of period 10^5 yr and with the sawtooth shape illustrated

in Fig. 4. This prehistory spans the last part of the Pleistocene geological epoch in which the the 10^5 yr cycle is most clearly present. The cross on Fig. 6 denotes the observed polar wander speed of magnitude $0.95°(\pm 0.15°)/10^6$ yr revealed by the ILS data shown in Fig. 1 (e.g. Dickman 1977). We have centred the observation at $t = 6$ kyr. This choice implies that the present epoch (in which the observation of polar wander speed is made) is a period of 11 kyr from the mid-point of the 10 kyr duration of the last of the model melting events. This provides a reasonable fit of the melting history of the ICE-2 model tabulated in Wu & Peltier (1983).

The results in Fig. 6 illustrate the impact of increased complexity of the basic elastic structure on the polar wander speed prediction. In each model the lithospheric thickness $\bar{L}$ is fixed at 120 km and the upper mantle viscosity ν_{UM} at 10^{21} Pa s. The models are all members of a sequence called LNF where the initial and final letters denote the presence of a lithosphere and that the elastic structure is a flat (F) approximation to that of 1066B (i.e. of the type shown in Fig. 5). The integer N denotes the number of internal density discontinuities in the mantle. Thus L0F (no core) is the homogeneous model shown by the dashed lines in Fig. 5 while L0F is model 1 in Fig. 5, L1F model 2, and L2F model 3. Although the speed prediction for L0F (no core) is not identically zero as was obtained for the homogeneous model in Section 3.1 the predicted speed is so slow that it does not show on the scale of the figure. That it differs at all from zero is a consequence of the fact that this model actually supports two separate modes of relaxation rather than one as assumed previously. However, the lithospheric mode is very weakly excited and the result thus shows that the general solution (81) converges to the previous homogeneous result in the appropriate limit. Introduction of a core into the model (L0F) leads to a marked increase in speed, as does the introduction of an internal density discontinuity into the mantle (L1F). The introduction of a second internal density discontinuity (L2F) does not further modify the instantaneous speed prediction significantly. It should be noted that all of these calculations have assumed the core to be inviscid and a constant mantle viscosity of 10^{21} Pa s. With this level of internal complexity the speed prediction exceeds the observed speed considerably but this discrepancy may be removed by increasing the viscosity of the lower mantle by about a factor of 3. The result for such a calculation is also shown in Fig. 6.

Although this fit to the data with $\bar{L} = 120$ km, $\nu_{UM} = 10^{21}$ Pa s and $\nu_{LM} \simeq 3 \times 10^{21}$ Pa s is attractive since it agrees (with respect to ν_{LM}) with previous analyses based on free air gravity data (Peltier & Wu 1982; Wu & Peltier 1983) the attraction is only superficial. This is because the polar wander speed prediction is as sensitive to lithospheric thickness as it is to ν_{LM} and so cannot be employed unambiguously to constrain the latter. The strength of the trade-off between $\bar{L}$ and ν_{LM} with ν_{UM} fixed at 10^{21} Pa s is illustrated by Fig. 7 on which is plotted the region of the $(\bar{L}, \nu_{LM})$ plane for which one may fit the observed polar wander speed within the observational error. The figure illustrates the trade-off as a function of t', the time since the mid-point of the last deglaciation event, and as a function of the number of previous cycles of the loading history. As is clear by inspection of this figure, unless we have independent knowledge of either $\bar{L}$ or ν_{LM} the datum is not a terribly useful one.

If we assume $\nu_{LM} \simeq 3 \times 10^{21}$ Pa s as required by previous analyses of free air gravity data and by the observed non-tidal acceleration of rotation (see Section 4) then the preferred value of $\bar{L}$ is about 120 km since the best fit t' is near 11.5 kyr. If we interpret $\bar{L}$ as a mean lithospheric thickness for the entire planet we may infer a value for the average thickness of the continental lithosphere LC from the expression $LC = 3\bar{L} - 2L0$ where L0 is the average thickness of oceanic lithosphere and it has been assumed that the surface is 1/3 continental and 2/3 oceanic. Since $L0 \sim 70$ km on the basis of seismic observations we infer a mean continental thickness of $LC \simeq 200$ km. This is somewhat smaller than the previously

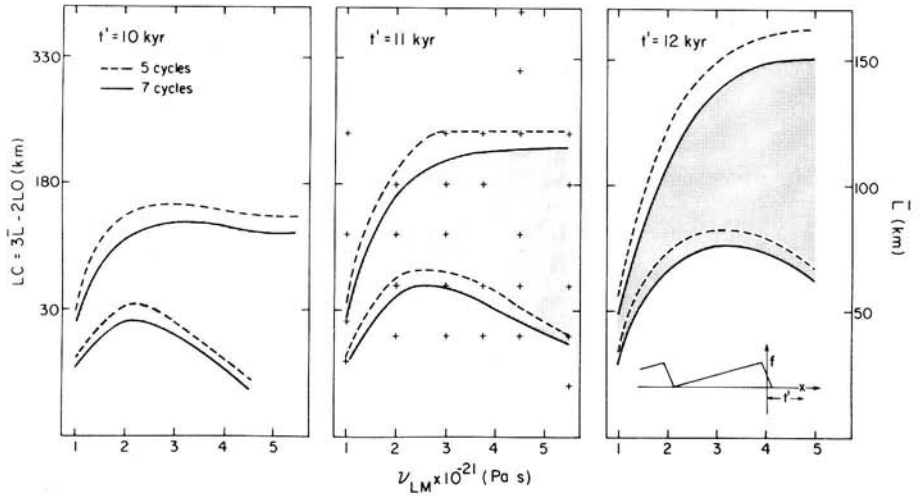

Figure 7. Trade-off curves between mean lithospheric thickness $\bar{L}$ and lower mantle viscosity ν_{LM}. The elastic structure is the 'flat' representation of 1066B and the upper mantle viscosity is held fixed at 10^{21} Pa s. The hatched region on each plate denotes the range of parameters for which one may fit the observed present-day polar wander speed within the observational error. The trade-off curves are drawn for three different choices t' of the mid-point of the last deglaciation event and for two different choices of the number of previous 10^5 yr cycles of glaciation.

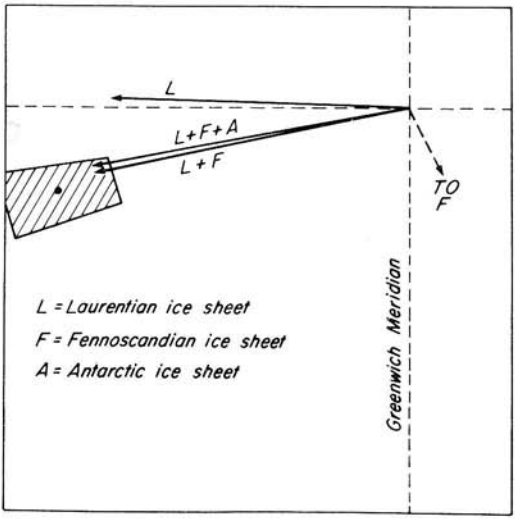

Figure 8. Variation of the direction and length of the polar wander velocity vector with the number of ice sheets employed in the loading history. The earth model has lithospheric thickness $\bar{L} = 120$ km, the upper mantle viscosity equals 10^{21} Pa s, and the lower mantle viscosity is 3×10^{21} Pa s.

reported value (Peltier & Wu 1983) of about 260 km for LC. This previous estimate was somewhat inaccurate due to a problem with the computation of the g_j defined in equation (67).

Fig. 8 illustrates the way in which the direction and length of the predicted polar wander velocity vector vary as the number of ice sheets employed in the simulation changes. Calculations are shown for the Laurentian region only (labelled L in the figure), for Laurentia and Fennoscandia (L + F), and including the effect of the melting event in

Antarctica (L + F + A). The observation is shown as the hatched region and it should be kept in mind that the earth model employed has a lower mantle viscosity of 3×10^{21} Pa s. Clearly the incorporation of the melting event in Fennoscandia is very important to the correct prediction of the direction of polar wander whereas the melting event on Antarctica has a very minor effect in spite of the considerable mass involved. The relative unimportance of the Antarctic melting event is simply due to the fact that it is located so near the rotation pole that it is very inefficient at exciting polar wander. It should be clear by inspection of the form of the general solution (81) that the direction of polar wander when $f = \dot{f} = 0$ may be simply determined from $\dot{\bar{m}}_2/\dot{\bar{m}}_1 = I^{\mathrm{R}}_{23}/I^{\mathrm{R}}_{13}$. In the last column of Table 3 we have therefore listed the angle of the predicted polar wander velocity vector wrt the x_1 direction. Note that the observed angle is $76^\circ \pm 5^\circ$ so that the predicted direction is well within the experimental error.

The results of this subsection show rather clearly that the observed speed of polar wander is a geophysical datum which is not unambiguously interpretable. It depends jointly upon the mantle viscosity profile and the thickness of the lithosphere. Only by fixing the mantle viscosity profile by appeal to other observations can we fix the model parameters in an unambiguous way. In Section 4 of this paper we will see that this defect is not shared by the observed non-tidal acceleration of planetary rotation. The next subsection will deal with the possibility that the cyclic glaciation and deglaciation of the polar continents which has characterized the Pleistocene period may produce a significant *net* wander of the rotation pole away from its pre-Pleistocene geographic location.

3.3 UNIDIRECTIONAL TRUE POLAR WANDER

In Fig. 4 we showed that during the ice age cycle the direction of motion of the rotation pole was away from the centre of glaciation during the glaciation phase and towards this location during the deglaciation phase. The question naturally arises as to what might be the average value of the speed over a single cycle, and whether, if this value is different from zero, there might be important physical effects expected as a consequence. In the recent papers by Sabadini *et al.* (1982a, b) it is claimed that this mean speed is very large indeed and could be responsible for a net displacement of the rotation pole during the Pleistocene period which is as large as 5° of latitude. These authors claim that this mechanism could explain the true polar wander allowed by palaeomagnetic observations. Here we will show that this estimate is at least a factor of 10 too large and therefore that the net drift of the rotation pole produced by cyclic loading is not likely to be of importance in so far as the palaeomagnetic data are concerned.

Inspection of equation (81) using the results of the Appendix shows that the predicted speed is dependent upon the number of previous cycles in the loading history. The average of $\dot{\bar{m}}_i$ over a glacial cycle, which we will denote by $\langle \dot{\bar{m}}_i \rangle$, will therefore be time dependent. From (81) we obtain

$$\langle \dot{\bar{m}}_j \rangle = \frac{\Omega}{A\sigma_0} I^{\mathrm{R}}_{j3} \left[D_1 \langle \dot{f} \rangle + D_2 \langle f \rangle + \sum_{i=1}^{N-1} E_i \left\langle \frac{d}{dt} f * \exp(-\lambda_i t) \right\rangle \right] . \tag{82}$$

With f the sawtooth function shown in Fig. 3 we have

$$\langle f(t) \rangle = 1/2 \tag{83a}$$

$$\langle \dot{f}(t) \rangle = 0 \tag{83b}$$

$$\left\langle \frac{d}{dt} f * \exp(-\lambda_i t) \right\rangle = \frac{\beta_1 \exp[\![-\lambda_i [\Delta t + M(\Delta T + \Delta t)]]\!]}{\lambda_i (\Delta T + \Delta t)} \tag{83c}$$

where β_1 is defined in the Appendix and M is the number of glacial cycles which have preceded the present one. In Fig. 9 we have plotted $\langle \dot{\tilde{m}}_j \rangle = \dot{\tilde{m}}$ as a function of M, the number of previous cycles, using viscoelastic model L2F.

We see that there are three basic regimes in the $\dot{\tilde{m}}$ history. Early in the history there is a large starting transient which decays slowly. After about 20 load cycles have been completed the rotation pole begins to drift at a very slow constant speed away from the centre of loading. At this time the net displacement realized is between 0.25 and 0.5°, depending upon the assumed value of the lower mantle viscosity. In the regime of steady drift which is approached at large M the magnitude of $\dot{\tilde{m}}$ is determined entirely by the second term in square brackets on the right hand side of (82) since the contribution from (83c) has decayed essentially to zero. Therefore the steady drift speed is given by

$$\langle \dot{\tilde{m}}_j \rangle = \frac{\Omega}{2A\sigma_0} I_{j3}^{R} D_2 . \tag{84}$$

But D_2, using (80) and (76) is just

$$D_2 = l_s \prod_{i=1}^{N} s_i \Big/ \prod_{i=1}^{N-1} \lambda_i . \tag{85}$$

Inspection of Table 4 shows that the D_2 are very small numbers which imply mean drift speeds of about $0.02°/10^6$ yr. The third phase in the $\tilde{m}$ histories shown in Fig. 9 is identified as the stopping transient. In computing this history we assumed that following 20 glacial cycles the climatic oscillation ceased. The stopping transient involves relatively large positive

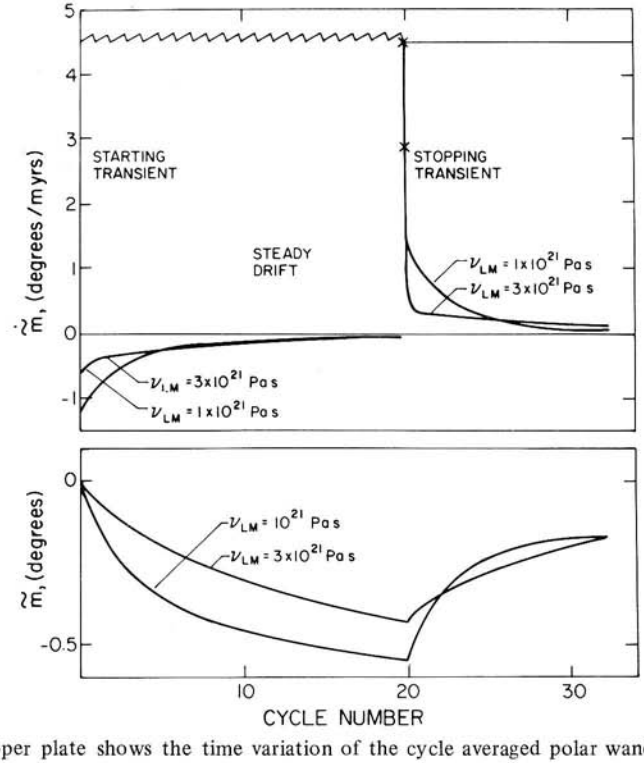

Figure 9. The upper plate shows the time variation of the cycle averaged polar wander velocity over a 20 cycle load history and the ensuing transient variation of speed after the cyclic loading ceases. The lower plate shows the net displacement of the rotation pole effected by this secular variation of polar wander speed. The net displacements expected are extremely small.

drift velocities compared to those which obtain in the starting transient phase. The net effect of the stopping transient is to shift the pole back towards the position it occupied prior to the commencement of the loading-unloading cycle.

Since the net shift of the pole is considerably less than 0.5°, even after 20 full cycles of loading, the amount of true polar wander which might have been produced by this mechanism is at least an order of magnitude smaller than that obtained by Sabadini *et al.* (1982a, b). The difference between the results of these two calculations appears to be due to the same mathematical error in the Sabadini *et al.* analysis of the layered model which we discussed previously. Since only about seven dominant cycles of duration 10^5 yr have occurred, the time prior to 7×10^5 yr BP being characterized by a much weaker form of this oscillation, the net displacement of the pole has probably been less than 0.25° during Pleistocene time. Since this represents a displacement of only about 10 miles it seems unlikely that it would be detectable in the palaeomagnetic record.

4 The non-tidal acceleration of rotation and $\dot{J}_2$

Our aim in past analyses of the polar wander observed in the ILS data shown in Fig. 1 was to employ this datum to provide an additional constraint upon the viscosity of the lower mantle. As we have seen here, however, the datum cannot be unambiguously interpreted in terms of this quantity because of the strong dependence of the predicted polar wander speed upon the thickness of the lithosphere. Fortunately the non-tidal acceleration of rotation is an observation which does provide the additional (and unambiguous) constraint which we are seeking. Published observations of this quantity are listed in Table 6. Although the observed variation of the Earth's rate of rotation, and thus of the length of day (lod), is strongly dominated by the torque exerted on the Earth by the dissipation of lunar oceanic tides in shallow seas, it has nevertheless proven possible to extract from the historical data a component which is not so explicable. If we assume that the ocean tidal torque has been constant over the past several thousand years, which is reasonable because the configuration of the oceans has been essentially fixed, then we may predict the time of occurrence of historical solar and lunar eclipses. Comparison of such predictions with the times of occurrence recorded in historical records shows that there is a systematic departure between theory and observation which is such as to imply the action of an acceleration (i.e. in opposition to the deceleration of rotation produced by lunar oceanic tides) in the amount recorded in Table 6. In this subsection we will show that this observed non-tidal acceleration is also understandable as an effect due to Pleistocene deglaciation and that it can be employed to provide a rather unambiguous constraint upon the viscosity of the lower mantle. We will also show that analyses of modern satellite orbital data provide us with a new method by which the inference of mantle viscosity from the non-tidal acceleration may be verified and made more accurate.

Table 6. Measurements of the non-tidal component of the acceleration of rotation.

Source	Value $(\dot{\omega}_3/\Omega)(\times 10^{-10}\,\mathrm{yr}^{-1})$
Currot (1966)	0.7 ± 0.3
Müller & Stephenson (1975)	1.5 ± 0.3
Morrison (1973)	2.9 ± 0.3
Lambeck (1977)	0.69 ± 0.3

The theoretical prediction of the acceleration of rotation due to ice sheet loading and unloading follows directly from equation (5), Laplace transformation of which yields

$$m_3(s) = -\frac{I_{33}(s)}{C} \tag{86}$$

where

$$I_{33}(s) = [1 + k_2^{\mathrm{L}}(s)]\, f(s)\, I_{33}^{\mathrm{R}} \tag{87}$$

and I_{33}^{R} is given by equation (13). If, as before, the ice sheets are approximated by circular disc loads and the ocean is described by the ocean function then I_{33}^{R} is given by equation (28). For a compressible, stratified, viscoelastic earth (61b) gives

$$1 + k_2^{\mathrm{L}}(s) = l_s - s \sum_j \frac{(r_j/s_j)}{(s + s_j)} \,. \tag{88}$$

Substituting (87) and (88) into (86), Laplace inversion of $m_3(s)$ gives

$$m_3(t) = -\frac{I_{33}^{\mathrm{R}}}{C} \left[\!\!\left[D_1 f(t) + \sum_j r_j [f * \exp(-s_j t)] \right]\!\!\right] . \tag{89}$$

Time differentiation of (107) then leads to the non-tidal acceleration

$$\dot{m}_3(t) = -\frac{I_{33}^{\mathrm{R}}}{C} \left[\!\!\left[D_1 \dot{f}(t) + \sum_j r_j \frac{d}{dt} [f * \exp(-s_j t)] \right]\!\!\right] . \tag{90}$$

The parameter D_1 is exactly that defined in (80). We will proceed to compare the theoretical prediction of (90) with the observations listed in Table 6. In making these comparisons we will again assume the ramp-shaped approximation to the glaciation history illustrated in Fig. 3. The convolution integrals $f * \exp(-s_j t)$ are then of the form given in the Appendix.

Before discussing our numerical results we will comment briefly upon the form of the solution (90). The first term describes the acceleration of rotation due to the direct effect of the load. During glaciation $\dot{f} > 0$ so that (since I_{33}^{R} is negative) this term tends to make $\dot{m}_3(t) > 0$. Since the accumulation of ice at the poles tends to reduce the polar moment of inertia, the rotation rate must increase in order to conserve angular momentum. During deglaciation, $\dot{f} < 0$, and the reverse is true. When the system is neither glaciating nor deglaciating then $\dot{f} = 0$ and only the second term, which clearly depends upon the glaciation history, may contribute to the acceleration of rotation. According to our past discussion we are apparently now living in such a time of near hiatus in the glaciation cycle and so we must rely upon the second term in (90) to fit the data listed in Fig. 6. When $f = \dot{f} = 0$, as is at least approximately true at present, it is clear that this term contributes a positive amount to the acceleration of rotation and so is at least capable in principle of explaining the observation.

In Fig. 10 we have plotted the predicted non-tidal acceleration of rotation for four stratified compressible viscoelastic earth models each of which has 1066B elastic structure. The models all have $\overline{L} = 120$ km and $\nu_{\mathrm{UM}} = 10^{21}$ Pa s while ν_{LM} is $(1, 3, 10, 100) \times 10^{21}$ Pa s for models 1, 2, 3 and 4 respectively. The theoretical results are shown as a function of time in kyr following the end of the last deglaciation event and again we have assumed that the glaciation history consists of 7 ramp-shaped loading events. All calculations include Laurentian, Fennoscandian and Antarctic melting events and the oceans are treated realistically. In Fig. 10 the observation labelled M is that of Morrison (1973) whose estimate is based upon lunar occultations over the period 1663–1972. That labelled M and S is from Müller & Stephenson (1975) who reanalysed the ancient eclipse data discussed by Newton

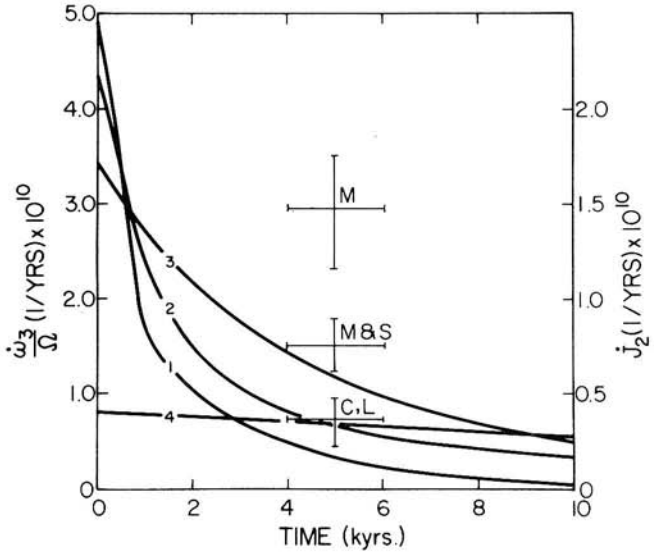

Figure 10. Predictions of the history of the non-tidal acceleration of rotation since the end of the last deglaciation event of a 7-cycle loading history for several different viscosity models discussed in the text. All calculations include Laurentian, Fennoscandian and Antarctic ice loads. The crosses denote observational estimates listed in Table 6 with that labelled C, L being the most accurate.

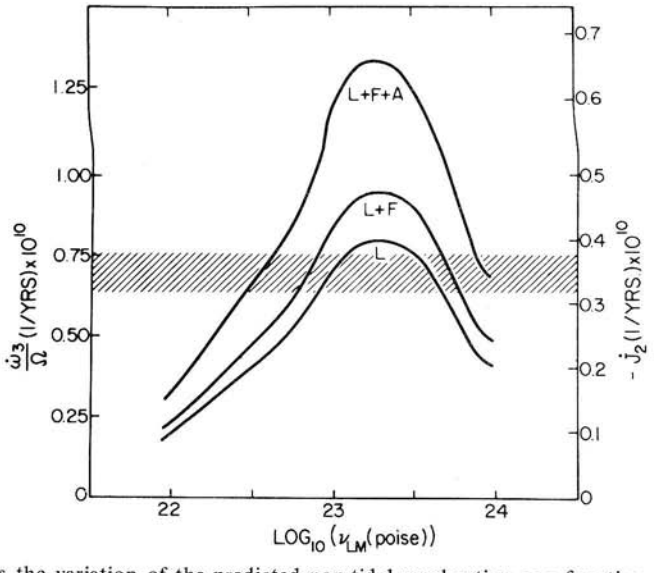

Figure 11. Shows the variation of the predicted non-tidal acceleration as a function of the viscosity of the lower mantle for models with fixed lithospheric thickness $L = 120$ km. Calculations are shown for loading by the Laurentian ice sheet only, for simultaneous Laurentian and Fennoscandian loading, and including the Antarctic ice sheet also. The calculations including all three ice sheets is the one which is to be compared to the observation which is shown as the hatched region and which corresponds to that labelled C, L in Fig. 10. Clearly there are two ranges of lower mantle viscosity allowed by the data and in order to resolve the ambiguity we must appeal to other observations.

(1972). The other observation is that by Currot (1966), marked C. The latter value was confirmed by Lambeck (1977) and we will accept it as the more accurate.

Inspection of Fig. 10 shows that as we increase the viscosity of the lower mantle from 10^{21} Pa s (model 1), to 3×10^{21} Pa s (model 2), to 10^{22} Pa s (model 3), to 10^{23} Pa s (model 4),

the acceleration predicted at $t = 0$ decreases and the decay time increases. This characteristic behaviour makes it possible to fit the observation with two widely spaced values of the viscosity of the lower mantle. This fact was first pointed out by SP whose one-layer analysis of the non-tidal acceleration is not influenced by the error made in connection with their analysis of polar wander. Fig. 11 shows more clearly the double root nature of the solution for lower mantle viscosity. The hatched region on this figure corresponds to the preferred value of the non-tidal acceleration (with error bars determined by the new LAGEOS data discussed in Peltier (1983) rather than by the analyses of ancient eclipse records indicated in Table 6) and the three curves show theoretical predictions for a model including only the Laurentian ice sheet, for a model including the Laurentian and Fennoscandian ice sheets, and for a model including the Laurentian, Fennoscandian and Antarctic ice sheets. Inspection of the figure shows that the Antarctic ice sheet is extremely important in so far as the non-tidal acceleration is concerned whereas it was relatively unimportant (see Fig. 8) as a source of excitation of polar wander. Again this is simply understood in terms of the polar location of the Antarctic ice mass. A given ice mass melting at the pole will contribute the largest possible change in I_{33}^{R} and thus will produce the largest possible $\dot{m}_3$.

The results of the calculation for all ice sheets which are shown in Fig. 11 demonstrate that it is possible to fit the observed non-tidal acceleration of rotation with two different families of models which differ from one another only in the magnitude of the viscosity of the lower mantle. All models have lithospheric thickness $L = 120.7$ km, an upper mantle viscosity of 10^{21} Pa s, and 1066B elastic structure. One group of models which fits the acceleration datum has the lower mantle viscosity ν_{LM} such that 2.7×10^{21} Pa s $\leqslant \nu_{LM} \leqslant 4.4 \times 10^{21}$ Pa s, whereas the other has 5×10^{22} Pa s $\leqslant \nu_{LM} \leqslant 1.5 \times 10^{23}$ Pa s. Only by invoking additional constraints can we decide which of these allowed values (or ranges of allowed values) is in fact correct. Fortunately such additional constraints exist. Recent analyses of relative sea-level and free air gravity data (Peltier 1981; Peltier & Wu 1982; Peltier 1982; Wu & Peltier 1982, 1983) have very clearly established that the viscosity of the lower mantle is bounded above by 10^{22} Pa s. Preferred models have a lower mantle viscosity in the vicinity of 3×10^{21} Pa s which is moderately in excess of the nominal 10^{21} Pa s upper mantle value. Clearly then only the smaller of the two families of lower mantle viscosity values allowed by the non-tidal acceleration datum is compatible with the relative sea-level and free air gravity data which we have analysed previously. It is extremely encouraging that the allowed range 2.7×10^{21} Pa s $\leqslant \nu_{LM} \leqslant 4.4 \times 10^{21}$ Pa s brackets the value of ν_{LM} preferred by these other data.

In the last section of this paper we showed that the polar wander datum was sensitive not only to the mantle viscosity profile but also to the lithospheric thickness L. In order to demonstrate that the non-tidal acceleration is not similarly sensitive to L we have computed $m_3(t)$ for a model which has $l = 295.3$ km rather than the value $L = 120.7$ km which is common to models 1–4. Analysis of the results for this model shows that varying L does not affect the model response significantly since $m_3(t)$ is only 3 per cent smaller than the prediction for model 1. The inference of ν_{LM} based upon the acceleration datum is therefore also insensitive to L.

In the remainder of this section we will demonstrate that there exists another geophysical observable, intimately related to the non-tidal acceleration of rotation, which may be employed to provide a further check upon the viscosity of the deep mantle inferred previously. This additional datum is the time derivative of the second-degree component of the Earth's gravitational potential field. We will hypothesize (as in Peltier 1982) that the dominant contribution to the time variation of this quantity is due to Pleistocene deglaciation and proceed to predict its magnitude. This quantity, usually referred to as $\dot{J}_2$,

may in fact be measured on the basis of the analysis of artificial satellite orbits from a sequence of successive temporal epochs (Yoder *et al.* 1983; Peltier 1983). As we will see, only the very accurate orbital data obtainable using satellite laser ranging are capable of actually observing the effect which we shall predict.

It is customary to write the spherical harmonic expansion of the gravitational potential perturbation in the form

$$\Delta\phi(\theta,\phi) = ag\left[\sum_{n=0}^{\infty} J_{n0} P_n^0(\cos\theta) + \sum_{n=1}^{\infty}\sum_{m=0}^{n} (J_{nm1}\cos\phi + J_{nm2}\sin\phi) P_n^m(\cos\theta)\right]. \quad (91)$$

If the cause of this perturbation of potential is due to loading of the Earth's surface by the surface mass density $\sigma(\theta', \phi')$ then the Laplace transform domain expression for $\Delta\phi$ may be written as

$$\Delta\phi(\theta,\phi) = \int_s\int G_\phi(\gamma)\,\sigma(\theta',\phi')\,a^2\sin\theta'\,d\theta'\,d\phi' \quad (92)$$

where $G_\phi(\gamma)$ is the Green function for the gravitational potential perturbation and γ is the angular distance between the field point (θ, ϕ) and the source point (θ', ϕ'). Peltier (1974) has shown that the function G_ϕ is

$$G_\phi(\gamma) = \frac{ag}{M_e}\sum_{n=0}^{\infty}(1+k_n^L)\,P_n^0(\cos\gamma) \quad (93)$$

where k_n^L is the load Love number of degree n. Making use of the addition theorem for spherical harmonics we may rewrite

$$G_\phi(\gamma) = \sum_{n=0}^{\infty} d_n^0 P_n^0(\cos\theta)\,P_n^0(\cos\theta') + \sum_{n=1}^{\infty}\sum_{m=1}^{n} d_n^m P_n^m(\cos\theta)\,P_n^m(\cos\theta')[\cos m\phi\cos m\phi' + \sin m\phi\sin m\phi'] \quad (94)$$

where

$$d_n^0 = \frac{ag}{M_e}(1+k_n^L) \quad (95a)$$

$$d_n^m = \frac{2ag}{M_e}\frac{(n-m)!}{(n+m)!}(1+k_n^L). \quad (95b)$$

If we also expand the surface mass density as in (11) then (92) becomes

$$\Delta\phi(\theta,\phi) = \sum_{n=0}^{\infty}\frac{4\pi a^3 g}{M_e}\frac{(1+k_n^L)}{(2n+1)}\sigma_{n01}P_n^0(\cos\theta) + \sum_{n=1}^{\infty}\sum_{m=1}^{n}\frac{4\pi a^3 g}{M_e}\frac{(1+k_n^L)}{(2n+1)}[\sigma_{nm1}\cos m\phi + \sigma_{nm2}\sin m\phi]\,P_n^m(\cos\theta). \quad (96)$$

Comparing (96) with (91) then yields

$$J_{nm_i}(s) = \frac{4\pi a^2}{M_e}\frac{[1+k_n^L(s)]}{(2n+1)}\sigma_{nm_i}(s). \quad (97)$$

Since realistic glaciation events conserve mass, $\sigma_{00} = 0$ and the dominant terms are those of second degree. Of particular importance is

$$J_{20}(s) = \frac{4\pi a^2}{5M_e}\,\sigma_{201}(s)[1 + k_2^L(s)]. \tag{98}$$

Assuming as before that $\sigma_{201}(t) = \sigma_{201} f(t)$, from (88) we have

$$J_2(t) = J_{20}(t) = \frac{4\pi a^2}{5M_e}\,\sigma_{201}\left[\left[D_1 f(t) + \sum_j r_j [f * \exp(-s_j t)]\right]\right] \tag{99}$$

and

$$\dot{J}_2(t) = \frac{4\pi a^2}{5M_e}\,\sigma_{201}\left[\left[D_1 \dot{f}(t) + \sum_j r_j \frac{d}{dt}[f * \exp(-s_j t)]\right]\right]. \tag{100}$$

Comparing (100) with (90) we observe that $\dot{m}_3(t)$ and $\dot{J}_2(t)$ are identical to within a constant. The relationship is such that

$$\dot{J}_2(t) = -\frac{4\pi a^2}{5M_e} \cdot \frac{C\sigma_{201}}{I_{33}^R} \cdot \dot{m}_3(t). \tag{101}$$

In Figs 10 and 11 we have made use of this relation to transform the predictions of $\dot{m}_3$ into predictions of $\dot{J}_2$, the units of which are shown adjacent to the right hand margin of the plots. We note that the predicted magnitude of $\dot{J}_2$ is about $10^{-10}\,\mathrm{yr}^{-1}$ which has just recently come within the accuracy of satellite laser ranging technology (Yoder *et al.* 1983). The availability of high quality satellite laser ranging data has recently made it possible to measure $\dot{J}_2$ rather accurately using the *LAGEOS* satellite and the observed $\dot{J}_2$ is shown as the hatched region in Fig. 11. The error bars on this measurement are reduced by more than a factor of 2 from those on the non-tidal acceleration obtained from ancient eclipse data and listed in Table 6. It is extremely interesting that the new observation of $\dot{J}_2$ from *LAGEOS* lies in the centre of the range estimated from the eclipse data. These new data have recently been discussed in Yoder *et al.* (1983) and Peltier (1983).

5 Conclusions

In this paper we have provided a new analysis of the influence of the Pleistocene glacial cycle upon the Earth's rotation. This analysis revealed important errors and inconsistencies in previous calculations of the polar motion produced by ice sheet forcing. Our main conclusion is that it is not possible to fit the observed polar wander in the ILS path with a homogeneous viscoelastic model of the planetary interior if a realistic cyclic history of glaciation and deglaciation is included in the calculation. This conclusion depends only in small part upon the assumption that we are currently living during a time of hiatus in a previously continuous load cycle (see Fig. 2). Neither does it appear to depend strongly upon the detailed nature of the load history during each cycle which is revealed in $^{18}O/^{16}O$ data from deep sea sedimentary cores. Although it is undoubtedly possible even with a perfectly elastic model of the internal rheology to choose a particular present-day rate of melting or accretion for Greenland and Antarctica such as to fit the observed polar wander (e.g. Munk & Revelle 1952) there is no independent evidence to our knowledge that any such effect is currently in progress.

Our analysis shows that when the viscoelastic stratification of the real Earth is taken into account in the calculation it is then possible to fit the observed magnitude and direction of

polar wander on the basis of the assumption that it is a memory of the last deglaciation event of the current ice age which ended prior to 5000 yr ago. In order to fit the observation with a model whose mantle viscosity profile is able simultaneously to reconcile the relative sea-level and free air gravity data of post glacial rebound (e.g. Peltier 1982), however, we were obliged to employ a lithospheric thickness in our model of approximately 120 km. If this number is interpreted as the average lithospheric thickness of the planet and if the oceanic average is assumed to be near 70 km the result implies a continental lithosphere thickness of about 200 km. This is in agreement with that inferred by Peltier (1984) on the basis of relative sea-level data from outside the Laurentian ice sheet margin.

The second rotational response to deglaciation which we explored was the change in the Earth's rate of spin. We showed that the astronomically observed non-tidal component of the acceleration of rotation was exactly of the magnitude expected on the basis of the hypothesis that it too is a memory of the planet of the last deglaciation event of the current ice age. Fortunately, this datum does not suffer from the same ambiguity of interpretation which afflicts the polar wander observation since the theoretical prediction is essentially independent of lithospheric thickness and a function only of mantle viscosity. Unfortunately, however, the inference of viscosity remains highly non-unique because one may trade-off the viscosity against the degree of initial isostatic disequilibrium and so fit the data with either one of two widely separated values of the mantle viscosity. The smaller of the two allowed roots for the viscosity of the lower mantle does agree very well, however, with the well constrained value which is determined by relative sea-level and free air gravity observations. This would appear to verify the hypothesis that the non-tidal acceleration has a glaciation cause.

A final idea which we investigated in this paper concerned the possibility that it might be possible to reinforce the above interpretation of the non-tidal acceleration of rotation through appeal to modern satellite orbital data. We showed that the non-tidal acceleration ω_{NT} was proportional to $\dot{J}_2$. Since J_2 itself is routinely retrieved from modern satellite tracking data it is in principle possible to measure $\dot{J}_2$ and thus to confirm the $\dot{\omega}_{NT}$ employed to constrain the mantle viscosity profile. This has in fact been accomplished very recently (Yoder *et al.* 1983, as discussed in Peltier 1983) with results predicted in Peltier (1982).

References

Currot, D. R., 1966. Earth deceleration from ancient solar eclipses, *Astr. J.*, **71**, 264–269.

Dickman, S. R., 1977. Secular trend of the Earth's rotation pole: consideration of motion of the latitude observatories, *Geophys. J. R. astr. Soc.*, **51**, 229–244.

Gilbert, F. & Dziewonski, A., 1975. An application of normal mode theory to the retrieval of structural parameters and source mechanisms from seismic spectra, *Phil. Trans. R. Soc. A*, **278**, 187–269.

Hays, J. D., Imbrie, J. & Shackleton, N. J., 1976. Variations in the Earth's orbit: pacemaker of the ice ages, *Science*, **194**, 1121–1132.

Kukla, G., Berger, A., Lotti, R. & Brown, J., 1981. Orbital signature of interglacials, *Nature*, **290**, 295–298.

Lambeck, J., 1977. Tidal dissipation in the oceans: astronomical, geophysical and oceanographic consequences. *Phil. Trans. R. Soc. A*, **287**, 545–594.

Lambeck, K., 1980. *The Earth's Variable Rotation: Geophysical Causes and Consequences*, Cambridge University Press, London.

McKenzie, D. P., 1967. The viscosity of the mantle, *Geophys. J. R. astr. Soc.*, **14**, 297–305.

McKenzie, D. P. & Weiss, N. O., 1975. Speculations upon the thermal and tectonic history of the Earth, *Geophys. J. R. astr. Soc.*, **42**, 131–174.

Morrison, L. V., 1973. Rotation of the Earth and the constancy of *G*, *Nature*, **241**, 519–520.
Müller, P. M. & Stephenson, F. R., 1975. The acceleration of the earth and moon from early observations, in *Growth Rhythms and History of the Earth's Rotation*, pp. 459–534, eds Rosenberg, G. D. & Runcorn, S. K., Wiley, New York.
Munk, W. H. & MacDonald, G. J. F., 1960. *The Rotation of the Earth*, Cambridge University Press.
Munk, W. H. & Revelle, R., 1952. On the geophysical interpretation of irregularities in the rotation of the Earth. *Mon. Not. R. astr. Soc., Geophys. Suppl.*, **6**, 331–347.
Nakiboglu, S. M. & Lambeck, K., 1980. Deglaciation effects on the rotation of the Earth, *Geophys. J. R. astr. Soc.*, **62**, 49–58.
Nakiboglu, S. M. & Lambeck, K., 1981. Corrections to 'Deglaciation effects on the rotation of the Earth', *Geophys. J. R. astr. Soc.*, **64**, 559.
Newton, R. R., 1972. *Medieval Chronicles and the Rotation of the Earth*, Johns Hopkins University Press, Baltimore.
Peltier, W. R., 1974. The impulse response of a Maxwell earth, *Rev. Geophys. Space Phys.*, **12**, 649–669.
Peltier, W. R., 1976. Glacial isostatic adjustment – II: the inverse problem, *Geophys. J. R. astr. Soc.*, **46**, 669–705.
Peltier, W. R., 1981. Ice age geodynamics, *Ann. Rev. Earth planet. Sci.*, **9**, 199–225.
Peltier, W. R., 1982. Dynamics of the ice age earth, *Adv. Geophys.*, **24**, 1–146.
Peltier, W. R., 1983. Constraint on deep mantle viscosity from Lageos acceleration data, *Nature*, **304**, 434–436.
Peltier, W. R., 1984. The thickness of the continental lithosphere, *J. geophys. Res.*, submitted.
Peltier, W. R. & Andrews, J. T., 1976. Glacial isostatic adjustment – I. The forward problem, *Geophys. J. R. astr. Soc.*, **46**, 605–646.
Peltier, W. R. & Jarvis, G. T., 1982. Whole mantle convection and the thermal evolution of the earth, *Phys. Earth planet. Int.*, **29**, 281–304.
Peltier, W. R. & Wu, Patrick, 1982. Mantle phase transitions and the free air gravity anomalies over Fennoscandia and Laurentia, *Geophys. Res. Lett.*, **9**, 731–734.
Peltier, W. R. & Wu, Patrick, 1983. Continental lithospheric thickness and deglaciation induced true polar wander, *Geophys. Res. Lett.*, **10**, 181–184.
Sabadini, R. & Peltier, W. R., 1981. Pleistocene deglaciation and the Earth's rotation: implications for mantle viscosity, *Geophys. J. R. astr. Soc.*, **66**, 553–578.
Sabadini, Roberto, Yuen, David A. & Boschi, Enzo, 1982a. Interaction of cryospheric forcings with rotational dynamics has consequences for ice ages, *Nature*, **296**, 338–341.
Sabadini, Roberto, Yuen, David A. & Boschi, Enzo, 1982b. Polar wandering and the forced responses of a rotating, multilayered, viscoelastic planet, *J. geophys. Res.*, **87**, 2885–2903.
Shackleton, N. J., 1967. Oxygen isotrope analyses and Pleistocene temperatures readdressed, *Nature*, **215**, 15–17.
Shackleton, N. J. & Opdyke, N. D., 1973. Oxygen isotrope and palaeomagnetic stratigraphy of equatorial Pacific core V28–238: oxygen isotrope temperatures and ice volumes on a 10^5 and 10^6 year time scale, *Quat. Res.*, **3**, 39–54.
Wu, Patrick & Peltier, W. R., 1982. Viscous gravitational relaxation, *Geophys. J. R. astr. Soc.*, **70**, 435–486.
Wu, Patrick, & Peltier, W. R., 1983. Glacial isostatic adjustment and the free air gravity anomaly as a constraint upon deep mantle viscosity, *Geophys. J. R. astr. Soc.*, **74**, 377–449.
Yoder, C. F., Williams, J. G., Dickey, J. O., Schutz, B. E., Eanes, R. J. & Tapley, B. D., 1983. $\dot{J}_2$ from *Lageos* and the non-tidal acceleration of earth rotation, *Nature*, **303**, 757–762.

Appendix

In the main text (e.g. equation 81) we showed that the solution for both the forced polar wander and the non-tidal acceleration of rotation of a glaciating earth contained terms involving the convolution of the load history $f(t)$ with decaying exponentials of the form $\exp(-\gamma t)$, as $f * \exp(-\gamma t)$. Since the glacial history may often be realistically approximated by a periodic sawtooth function of the form shown in Fig. 3, we are required to evaluate the convolution integrals in this specific case.

For a single cycle of such a sawtooth history we may write $f(t)$ as

$$f(t) = \frac{(t-a)}{(b-a)}, \qquad \text{for } a \leqslant t \leqslant b$$

$$= \frac{(t-c)}{(b-c)} \qquad \text{for } b \leqslant t \leqq c$$

$$= 0 \qquad \text{otherwise}$$

then

$$f * \exp(-\gamma t) = \int_a^t f(t') \exp[-\gamma(t-t')]\, dt'$$

$$= \exp(-\gamma t) \int_0^t f(t') \exp(\gamma t')\, dt' \qquad \text{by definition.} \tag{A1}$$

Evaluation of (A1) is straightforward and yields

$$f * \exp(-\gamma t) = 0 \qquad t \leqslant a$$

$$= \frac{1}{\gamma}\left[\frac{(t-a)}{(b-a)} + \frac{\exp[-\gamma(t-a)] - 1}{\gamma(b-a)}\right] \qquad a \leqslant t \leqslant b$$

$$= -\frac{1}{\gamma}\frac{\exp[-\gamma(t-b)] - 1}{\gamma(b-c)} + \frac{\exp[-\gamma(t-a)] - \exp[-\gamma(t-b)]}{\gamma(b-a)} + \frac{(t-c)}{(b-c)}$$

$$b \leqslant t \leqslant c$$

$$= \frac{\exp[-\gamma(t-b)]}{\gamma}\left[\frac{\exp[-\gamma(b-a)] - 1}{\gamma(b-a)} + \frac{\exp[\gamma(c-b)] - 1}{\gamma(c-b)}\right] \qquad t \geqslant c.$$

The time derivative of this expression is also useful and is given by

$$\frac{d}{dt}[f * \exp(-\gamma t)] = 0 \qquad t \leqslant a$$

$$= \frac{[\![1 - \exp[-\gamma(t-a)]]\!]}{\gamma(b-a)} \qquad a \leqslant t \leqslant b$$

$$= \frac{[\![1 - \exp[-\gamma(t-b]]\!]}{\gamma(b-c)} + \frac{\exp[-\gamma(t-b)] - \exp[-\gamma(t-b)]}{\gamma(b-a)}$$

$$b \leqslant t \leqslant c$$

$$= -\exp[-\gamma(t-b)]\left[\frac{\exp[-\gamma(b-a)] - 1}{\gamma(b-a)} + \frac{\exp[\gamma(c-b)] - 1}{\gamma(c-b)}\right]$$

$$c \leqslant t. \tag{A3}$$

For the case in which there are N loading cycles of this form we may simplify the expression for the solution by defining $\Delta T = b - a$ as the duration of the loading phase of the cycle and $\Delta t = c - b$ as the duration of the unloading phase. On the basis of (A3) we may then note that the effect of the previous cycle at the time t is just $\beta_1(\gamma) \exp[-\gamma(t-b)]/\gamma$ where

$$\beta_1(\gamma) = \left[\frac{\exp(-\gamma\Delta T) - 1}{\gamma\Delta T} + \frac{\exp(\gamma\Delta t) - 1}{\gamma\Delta t}\right]. \tag{A4}$$

The effect of the kth previous cycle will be just $\beta_1(\gamma) \exp\{-\gamma[t-b+k(\Delta T + \Delta t)]/\gamma\}$ since this cycle is just time shifted by the amount $k(\Delta T + \Delta t)$. The effect of N previous cycles is then just

$$S = \sum_{k=0}^{N-1} \beta_1(\gamma) \exp[-\gamma(t-b)] [\![\exp[-\gamma(\Delta T + \Delta t)]]\!]^k/\gamma \tag{A5}$$

which may be assumed exactly as a geometric series to give

$$S = \frac{\beta_1(\gamma) \exp[-\gamma(t-b)]}{\gamma} \frac{[\![1 - \exp[-\gamma N(\Delta T + \Delta t)]]\!]}{[\![1 - \exp[-\gamma(\Delta T + \Delta t)]]\!]} = \beta_N \frac{\exp[-\gamma(t-b)]}{\gamma}. \tag{A6}$$

Since the response at time t is simply the sum of this effect of this past cycle and the convolution representing the effect of the present (Nth) cycle we have a very simple expression for the general solution. If $t = b$ defines the time of the most recent glacial maximum the present cycle starts at $t = b + \Delta t$, reaches maximum at $t = b + \Delta t + \Delta T$ and we may write:

(1) During the glaciation phase

$$f * \exp(-\gamma t) = \beta_N(\gamma) \frac{\exp[-\gamma(t-b)]}{\gamma} + \frac{[\![\gamma(t-b-\Delta t) + \exp[-\gamma(t-b-\Delta t)] - 1]\!]}{\gamma^2 \Delta T} \tag{A7}$$

$$\frac{d}{dt}[f * \exp(-\gamma t)] = -\beta_N(\gamma) \exp[-\gamma(t-b)] + \frac{[\![1 - \exp[-\gamma(t-b-\Delta t)]]\!]}{(\gamma\Delta T)}. \tag{A8}$$

(2) During the deglaciation phase

$$f * \exp(-\gamma t) = \beta_N \frac{(\gamma) \exp[-\gamma(t-b)]}{\gamma} + \frac{1}{\gamma}\left[\frac{1 - \exp[-\gamma(t-b-\Delta t-\Delta T)]}{\gamma\Delta T} + \frac{\exp[-(t-b-\Delta t)] - \exp[-(t-b-\Delta t-\Delta T)]}{\gamma\Delta T} - \frac{(t-b-2\Delta t-\Delta T)}{\Delta t}\right] \tag{A9}$$

$$\frac{d}{dt}[f * \exp(-\gamma t)] = -\beta_N(\gamma) \exp[-\gamma(t-b)] + \exp[-\gamma(t-b-\Delta t)] \times \left[\frac{\exp(\gamma\Delta T) - \exp[+\gamma(t-b-\Delta t)]}{\gamma\Delta t} - \frac{[1 - \exp(-\gamma\Delta T)]}{\gamma\Delta T}\right]. \tag{A10}$$

Following the Nth cycle, at a time (like today) when the system is not subject to a surface load, we have:

(3) After loading has ceased

$$f * \exp(-\gamma t) = \beta_N(\gamma) \exp[-\gamma(t - b)]/\gamma \tag{A11}$$

$$\frac{d}{dt}[f * \exp(-\gamma t)] = -\beta_N(\gamma) \exp[-\gamma(t - b)]. \tag{A12}$$

The above relations are required in the numerical evaluation of the solutions presented in the main body of this paper.